NIST-GCR-98-747

Fire Detection Using Reflected Near Infrared Radiation and Source Temperature Discrimination

A.C. Lloyd, Y.J. Zhu, L.K. Tseng,
J.P. Gore and Y.R. Sivanthanu
Thermal Sciences and Propulsion Center
School of Mechanical Engineering
Purdue University
West Lafayette, IN 47909

United States Department of Commerce
Technology Administration
National Institute of Standards and Technology

NIST-GCR-98-747

Fire Detection Using Reflected Near Infrared Radiation and Source Temperature Discrimination

Prepared for
U.S. Department of Commerce
National Institute of Standards and Technology
Gaithersburg, MD 20899

By
A.C. Lloyd, Y.J. Zhu, L.K. Tseng,
J.P. Gore and Y. R. Sivanthanu
Thermal Sciences and Propulsion Center
School of Mechanical Engineering
Purdue University
West Lafayette, IN 47907

October 1997
Issued April 1998

Notice

This report was prepared for the Building and Fire Research Laboratory of the National Institute of Standards and Technology under grant number 60NANB5D0113. The statement and conclusions contained in this report are those of the authors and do not necessarily reflect the views of the National Institute of Standards and Technology or the Building and Fire Research Laboratory.

Abstract

A new type of near infrared (NIR) fire detector which utilizes a statistical analysis of apparent source temperatures of fires was developed. The NIR fire detector measures the spectral radiation intensities emanating from fires at 900 and 1000 nm. These measurements are used to obtain and a time series of apparent source temperatures. The near infrared radiation characteristics of five standard test fires specified in the guidelines of the European Committee for Standardization were measured and utilized to develop a fire detection algorithm. The five test fires specified in the guidelines involved a heptane pool, a polyurethane foam, a wooden crib, a smoldering cotton and a smoldering wood. The normalized power spectral density of the spectral radiation intensity at 900 or 1000 nm combined with the probability density function of the apparent source temperatures are sufficient to determine the presence of the test fires in the vicinity of the detector. The NIR fire detector was evaluated for sensitivity to both direct and reflected radiation from the five test fires. When direct radiation is incident on the NIR fire detector, four of the five test fires were always detected. The smoldering wood fire was detected only if the NIR fire detector was very close. The NIR fire detector can also detect the heptane pool, the polyurethane foam and the wooden crib fires from reflected radiation. The response time of the NIR fire detector ranged from approximately 1 to 4 minutes for the open fires. The NIR fire detector had no instances of false alarms during the test period. The response time can be shortened considerably (to a few seconds) by using a programmable DSP chip rather than a personal computer. We continue to seek SBIR funding for developing this faster version.

A numerical technique based on the Discrete Probability Function (DPF) method in conjunction with a ray tracing algorithm was developed to handle radiative heat transfer problems in rectangular and cylindrical enclosures without participating media. The numerical technique has potential to assist building designers to find the optimal detector location for multiple room monitoring. The DPF method is much more accurate than conventional Monte Carlo methods for solving the surface radiative heat transfer problems studied in this project. The numerical evaluation confirmed that the detector can successfully detect fires from reflected radiation if its sensitivity is sufficiently high.

Acknowledgment

This research was supported by the United States Department of Commerce, National Institute of Standards and Technology (Grant No. 60NANB5D0113), with Dr. William Grosshandler serving as Scientific Officer. The authors wish to acknowledge the technical contributions of Dr. Roger Davis of Purdue University.

Table of Contents

List of Figures

Nomenclature

Symbol	Description
c	Velocity of light, m/s
E	Spectrum function, s
E_N	Normalized spectrum function
f	frequency
$f(\phi)$	Probability density function of variable ϕ
h	Planck's constant
I	Radiation intensity
k	Boltzmann constant
L	Length of the tube
M	Sampling frequency
N	Number of bins in the DPF of position
$P(\phi)$	Discrete probability function of variable ϕ
R	Radius of the tube
R(t)	Auto-correlation coefficient
l, m, n	Direction cosines
r	Radial coordinate
t	time
T	Temperature, K
x	Axial coordinate

Greek

ε	emissivity
ϕ	Azimuthal angle
μ	Cosine of the polar angle
θ	Polar angle
ρ	Hemispherical reflectivity
ρ_s	Hemispherical specular reflectivity
ρ_d	Hemispherical diffuse reflectivity
λ	Wavelength

Subscripts

b	blackbody
i, j, k	subscripts for bin values
λ	Wavelength
λ_1	First measurement wavelength (1000 nm)
λ_2	Second measurement wavelength (900 nm)

1. Introduction

The ability to detect fires in residential and industrial venues has been and will continue to be of the utmost importance. In 1995 alone, public fire departments responded to 1.965 million fires (Krater, 1996). 573,500 of these fires were structure fires resulting in $7.62 billion dollars in property damage. Seventy four percent, or 425,500, of these fires occurred in residential properties causing $4.363 billion in damage. More important than monetary concerns, fires also claimed 4,585 civilian lives and injured an additional 25,775. The number of fire deaths in the home rose 6.3% in 1995 to 3,640, accounting for 79% of all fire deaths. An additional concern is false alarms. It is estimated that 95% of all alarms from smoke detectors in the U. S. during the 1980's were unnecessary (Hall, 1989).

New fire detection concepts and algorithms are justified only if they improve upon existing ones with lower false alarm rates and greater sensitivity to starting fires. In addition, the detectors and signal processing instruments should be easy to operate and maintain, have high flexibility and be relatively inexpensive (Luck, 1992). Currently residential fire detectors include optical smoke sensors, ionization smoke sensors and temperature sensors (Grosshandler, 1992).

Conventional smoke sensors utilize light scattering or smoke ionization measurements to detect a fire, while temperature sensors utilize thermocouple measurements. The are three disadvantages with conventional single sensor detectors: (1) there is a significant time delay between the start of the fire and the transport of the combustion products to the location where the detector is mounted; (2) in instances when there are impermeable barriers (such as smoldering inside walls), the fire is not easily detected even in advanced stages, and; (3) single sensor detectors involve a high rate of false alarms due to changes in the operating environment. Combinations of smoke sensors and odor sensors which involve multiple fire signatures are less prone to false alarms (Okayama et al., 1994). However, multiple sensors involve greater construction cost and increased complexity of signal processing hardware and software.

More recently, there has been increased interest in the use of radiation emission sensors (flame detectors) as an alternative to smoke and heat sensors (Middleton, 1989). The three major advantages of emission sensors are: (1) their ability to survey the entire room for fire initiation, (2) their fast response time, and (3) false signals can be readily distinguished since most fires are unsteady with unique frequency content, leading to unambiguous discrimination based on the power spectral density of the measured intensities (Grosshandler, 1992).

Single channel flame detectors operate either in the ultraviolet (where solar radiation is totally absorbed by the earth's atmosphere) or in the infrared (where flame emission is primarily from hot CO_2) parts of the spectrum. Ultraviolet signals from flames are normally very low leading to false alarms from indoor radiation sources such as incandescent lights, arc welding processes, etc. Therefore, ultraviolet sensors are limited to outdoor usage where interfering solar radiation is absorbed by the earth's atmosphere. Another disadvantage of ultraviolet flame detectors is that any contamination of the optical windows causes a significant loss of sensitivity.

Infrared flame detectors are used for large indoor areas such as aircraft hangars and warehouses where direct solar radiation is minimal. Single channel infrared detectors look for radiation emitted from hot CO_2 gases present in most flames at wavelengths around 2.7 μm or 4.4 μm. These single channel detectors have precision band-pass optical filters in front of them to detect fires while successfully rejecting solar radiation. The major problem with single channel detection is that since only one channel of information is present, the chances of false alarms are relatively high (Okayama et al., 1994; Middleton, 1989).

The false alarm problems present with single channel detection can be partially alleviated by using two channels of information. Typically two-channel flame detectors use one channel in the infra-red (typically at 4.4 μm) to detect hot combustion products. The second channel is chosen above or below the 4.4 μm band where there is a high level of solar radiation coupled with low levels of flame radiation. The addition of the second channel is purely for the prevention of false alarms by rejecting interference (such as direct solar radiation) from a continuum source that does not have the ubiquitous 4.4 μm CO_2 band. Fire is still detected using the 4.4 μm infrared channel, and in cases where fire is present along with the interfering source, it might be difficult to resolve the signal unambiguously (Middleton, 1989). Further, highly luminous fires may go undetected if the detector is tuned to non-luminous fires. Commercial production of single channel infrared flame sensors which are insensitive to solar radiation, or a combination ultra-violet/infrared and even two-channel infrared flame sensors has been initiated for use in industrial applications (Middleton, 1989).

A fiber optic fire sensor that uses correlation between radiation at two wavelength spaced far apart in the visible to 2.0 micron wavelength band has been recently utilized to detect diesel fires (Wetzork et al., 1992). The fiber optic fire sensor utilizes the high degree of correlation between the intensities at the two wavelengths to provide immunity to false alarm sources. However details regarding the hardware of the fiber optic fire sensor or the fire detection algorithm were not reported.

The two most distinguishing features of a natural fire, particularly a luminous one, are its apparent source temperature and the power spectral density of the radiation intensities emitted from it. Two-wavelength pyrometric measurements conducted in luminous pool and jet fires (Sivathanu and Faeth, 1990; Sivathanu et al., 1991; Sivathanu and Gore, 1991) indicate that the peak temperatures within these fires are in the range 1400 ± 300K. The power spectral density of natural fires show a wide range of frequency present in them.

The additional advantage of utilizing radiation for fire detection is that the sensor can be placed away from the direct view of the fire. This allows multiple room monitoring with a single fire detector. However in arbitrarily shaped residential and commercial buildings, it is difficult to determine the right location for the placement of the fire detector. Typically, the fire detector should be located in places where the intensity incident on the detector is at a maximum. Design procedures for optimal placement of fire detectors have not been developed so far. For evaluation and eventual utilization of infrared radiation based fire detectors in residential and commercial buildings, a design tool is needed.

The calculation of radiative transfer in enclosures with and without participating media is of particular interest in developing such design tools for all radiation based fire detectors. Solutions to the equation of radiative transfer in enclosures have been obtained using a wide variety of methods. Pioneering computations (Hottel, 1954; Oppenheim, 1956; and Sparrow et al., 1961) involved solutions to the radiative transfer equations for diffuse surfaces. Eckert and Sparrow (1961) pioneered the use of the angle-factor method for analyzing radiative transfer in enclosures with specular surfaces. Subsequently different approximate methods based on extensions of the angle factor or the script-F method have been used to analyze radiative transfer in enclosures having specular and diffuse surfaces (Sparrow et al., 1962; Bobco, 1964; Bevans and Edwards, 1965; and Sarofim and Hottel, 1966). In addition, analytical methods for the calculation of radiative heat transfer for simple surfaces such as cylindrical and conical cavities (Lin and Sparrow, 1965) and axisymmetric passages (Rabl, 1977; and Mahan et al., 1979) have been developed.

Statistical methods for the calculation of radiative heat transfer in enclosures using Monte Carlo simulations have been published a few decades ago (Howell and Perlmutter, 1964; and Perlmutter and Howell 1964). Initially, unbiased or Direct Monte Carlo (Corlett, 1966; and Toor and Viskanta, 1968) simulations were used to calculate the thermal radiation in enclosures with mixed specular/diffuse surfaces. A review of the earlier Monte Carlo simulations of radiative transfer problems is found in Howell (1968).

Direct Monte Carlo methods are computer intensive, and therefore fully vectorized or parallelized codes are very helpful in reducing the costs associated with long run times. Monte Carlo algorithms for an irregular enclosure with arbitrary values for surface properties (transmitivity, specular and diffuse reflectivity) have been implemented using fully vectorized codes (Burns and Pryor, 1989). The accuracy and convergence of direct Monte Carlo algorithms have been documented (Maltby and Burns, 1991). A grid shading algorithm (Burns and Pryor, 1989) was shown to reduce computational time significantly. For complex 2-D and 3-D heat transfer problems, similar changes in the photon tracking kernel are necessary to obtain reasonable computational efficiency, and the authors (Burns and Pryor, 1989) suggested a weighted moving average process to reduce the number of photon trajectories required in such calculations.

There are several methods of reducing the sample size in Monte Carlo methods such as importance sampling and correlation and statistical estimation techniques (Kahn and Marshall, 1953). For radiative transfer calculations, weighting and biasing individual photons (Lanore, 1971) and importance sampling in conjunction with angular discretization (Burgart and Stevens, 1970) have been shown to reduce the computational time and increase accuracy for deep penetration problems.

Other schemes for improving accuracy such as the energy partition method (Shamsundar et al., 1972; and Modest, 1978) have been used to combine deterministic elements with a Monte Carlo simulation of radiative transfer calculations. Haji-Sheikh (1988) and Burns et al. (1990) provide a detailed literature review of the more recent Monte Carlo simulations of radiative transfer. Haji-Sheikh (1988) provides a very thorough exposition of the importance sampling method in radiative heat transfer problems for variance reduction. Monte Carlo methods are

currently being used in a variety of problems demonstrating their applicability for irregular shapes (Parthasarathy et al., 1994), discrete arrays (Drost and Welty, 1992), diffuse and specular reflectance and transmittance in axisymmetric enclosures (Burns et al., 1992). Recent papers (Tong and Skocypec, 1992) have shown that application of similar Monte Carlo approaches to a bench-mark problem can result in differences in solutions by a factor of 2 to 3.

Markov chain theory (Naraghi and Chung, 1984; and Billings et al., 1991) has been used to calculate the radiation interchange in enclosures with a finite number of isothermal diffuse and specular surfaces. Similar to the exodus modification of the Monte Carlo method (Emery and Carson, 1968), Markov chain theory does not need random number generators, eliminating one source of statistical fluctuations in the solutions. For single parameter state definition of the Markov chains, the calculation of the transition probability matrix for multiply (more than twice) reflected photons or for arbitrarily varying specular reflectivity proves to be challenging. A two parameter state definition in conjunction with the Markov chain method (Billings et al., 1991) makes it easier to treat specular reflections in enclosures. Billings et al. (1991) modeled the radiative heat transfer in a 2-dimensional square enclosure using this method. The biggest advantage of the Markov chain method is the ability to reuse the probability transition matrix.

Recently, to address the disadvantages associated with the use of random number generators in the Monte Carlo methods, we developed a Discrete Probability Function (DPF) method to calculate the spectral radiation intensity leaving a representative path in a flame (Sivathanu and Gore, 1993). The DPF method involves discretization of the probability density functions (PDFs) of the initial and boundary conditions of a variable into a finite number of bins (histogram representation). The governing equations are then applied to the individual bin values. Application of the governing equations to individual bin values is similar to their application to randomly selected values in the Monte Carlo method. In the DPF method, the values and probabilities associated with the solutions of the governing equations obtained are rebinned to provide the PDF of the solution. In the Monte Carlo method, the random sampling algorithm selects more of the higher probability values and less of the lower probability values of the initial and boundary conditions and source functions. The application of the governing equations to the resulting realizations leads to solutions that upon binning yield their PDF.

The DPF method was subsequently applied to the calculation of the view factors in a cylindrical tube with diffusely reflecting surfaces (Sivathanu and Gore, 1994). The computational cost of carrying the information concerning the probabilities was found to be less than that of considering a large number of random realizations required for Monte Carlo calculations in these two applications (Sivathanu and Gore, 1993, Sivathanu and Gore, 1994).

Based on the background information provided above, the objectives of the present project were: (1) to characterize the near infrared radiation intensities emanating from standard test fires, and (2) to develop numerical methods for the calculation of spectral radiation intensities incident on detectors from fires in arbitrarily shaped enclosures. The experiments and numerical simulations will be used to evaluate a near infrared fire detector, specifically suited for monitoring multiple room enclosures.

2. Experimental Evaluation

2.1 Principle of Operation

The principle of operation of the near-infrared fire detector is similar to the two-wavelength optical pyrometer used for determining soot volume fractions and temperatures in laboratory scale fires (Sivathanu et al., 1991). The spectral radiation intensity emitted by a source at any wavelength can obtained from the equation of radiative transfer as:

$$I_\lambda = \varepsilon_\lambda I_{\lambda b} \tag{2.1}$$

where $I_{\lambda b}$ is the blackbody intensity at the unknown source temperature T and ε_λ is its apparent spectral emissivity.

For fire detection, the exact temperature and the emissivity of the source is not of great importance. Rather, the existence of high temperatures in the vicinity of the detector is sufficient to indicate the presence of a fire. Therefore, the spectral emissivity of any radiation source (either direct or reflected) can be assumed to vary inversely with wavelength irrespective of its chemical composition, or the spectral reflectivity of intervening material. Using this assumption, the apparent temperature of any source, determined from the measured spectral radiation intensities at two wavelengths can be defined as:

$$T = \frac{hc}{k}\left(\frac{1}{\lambda_1} - \frac{1}{\lambda_2}\right) / \ln\left\{\left(\frac{\lambda_2^6}{\lambda_1^6}\right)\left(\frac{I_{\lambda 2}}{I_{\lambda 1}}\right)\right\} \tag{2.2}$$

where h is the Planck's constant, k is the Boltzmann constant, and c is the speed of light. The advantage of using two wavelengths close to one other is that the assumption of $1/\lambda$ dependence for the emissivity of the source does not introduce a very large error on the apparent source temperatures obtained using Eq. (2.2).

A schematic diagram of the near-infrared (NIR) fire detector is shown in Fig. 1. The fire

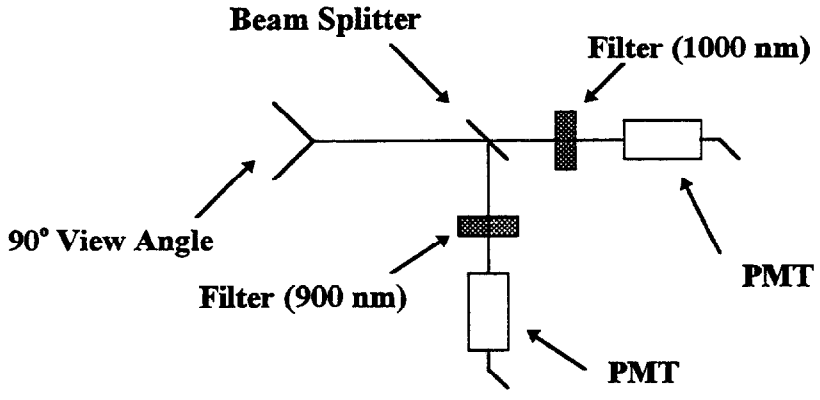

Figure 1. Schematic diagram of the NIR fire detector.

detector consists of 90^0 view angle optics that collect and collimate the radiation intensity incident on it. The collimated radiation intensity is split into two parts which are incident on two photo multiplier tubes (PMTs) that have narrow band pass filters (10 nm FWHM) centered at 900 and 1000 nm in front of them. The output voltages of the two PMTs were monitored using an A/D board and a laboratory computer. These voltages were converted to spectral radiation intensities using calibration constants obtained with a reference blackbody maintained at 1100 K.

The peak spectral radiation intensities in typical luminous fires such as acetylene and ethylene are at approximately 1500 nm (Gore, 1986). The intensities at 1000 nm are approximately a factor of three to four lower than at 1500 nm. However, there are three advantages to utilizing the spectral radiation intensities at 900 and 1000 nm rather than in the infrared regions to obtain apparent source temperatures: (1) near infrared fire detectors are less expensive, more sensitive and less prone to degradation than infrared detectors, (2) the sensitivity of the two-wavelength pyrometric technique to temperature is more when the wavelengths are close together and well shifted from the peak of the Planck function, and (3) building materials are much more reflective at 900 and 1000 nm than at 1500 nm, making detection of reflected radiation easier. The lower sensitivity of the infrared detectors could be alleviated to some extent by utilizing broader bandwidth optical filters in lieu of the 10 nm filter used here. However, the detector will have higher false alarm rates due to the lower rejection of environmental radiation. For the characterization studies reported in the following, the choice of 900 nm and 1000 nm wavelengths is close to the optimal, providing both a higher sensitivity to temperatures and an increased immunity to false alarms.

The spectral radiation intensities at 900 nm and 1000 nm incident on the two photo multiplier tubes were measured at 100 Hz. From the spectral radiation intensities, a time series of apparent source temperatures was obtained using Eq. (2). The time series of spectral radiation intensities and apparent source temperatures were analyzed to obtain their Probability Density Functions (PDF) and Power Spectral Densities (PSD).

2.2 Description of Standard Test Fires

Fire detectors commonly used in residential and commercial buildings are tested using six standard fires specified in the European Committee for Standardization (CEN, 1982) guidelines. Five of these standard fires are luminous. The sixth one is a non-luminous alcohol fire which cannot be detected by the present fire detector. The near-infrared radiation characteristics of the five luminous fires were studied to develop an effective fire detection algorithm.

A brief description of the five test fires is included in the following section. Some of the dimensions of the fires specified in the CEN (1982) guidelines were scaled down so as to be able to accommodate them in our laboratories. The open cellulosic fire (designated TF1 in the CEN (1982) guidelines) consisted of seven stacks of beechwood sticks arranged to form a wooden crib. Each stack consisted of three beechwood sticks of dimension 1 cm x 2 cm x 25 cm. The beechwood sticks were arranged in a cross layer pattern to form a square wooden crib 250 mm on each side. The wooden crib fire was ignited with 5 cm^3 of methylated spirit placed at the center.

The smoldering pyrolysis fire (designated TF2) consisted of 24 dried beechwood sticks arranged along the twelve radii of a grooved hot plate 220 mm in diameter. The beechwood sticks were 1 cm x 2 cm x 3.5 cm, and the hot plate was powered using a variable voltage controller so as to reach of temperature of 600 ^{o} C in 11 minutes. The wood smolders at approximately 8 minutes. The radiation from the hot plate is very high and therefore a radiation shield was used to prevent the detector from directly viewing the hot plate. During the characterization tests, which lasted approximately 3 minute, a flame was not present.

The glowing smoldering fire (designated TF3) consisted of 90 cotton wicks, 80 cm long, fastened by a wire ring 10 cm in diameter at one end. To maintain a cylindrical shape for the cotton wicks, they were wetted with water and allowed to dry in a current of air, while a small tension was applied at the other end. The cotton wicks were ignited using a propane torch. The flame were put out immediately after ignition, and the cotton wicks continued to glow for a long time.

The open plastics fire (designated TF4) consisted of 3 mats of soft polyurethane foam stacked one on top of another. The mats were 15 cm in diameter and 25 mm in height. The polyurethane foam has not been treated with any flame retarding additives and therefore is very flammable. The bottom mat was ignited at one corner and the flame spreads very rapidly, with the entire fuel being consumed in approximately 1 minute.

The liquid fire (designated TF5) consisted of a n-heptane pool fire stabilized on a water-cooled 15 cm diameter stainless steel burner. The height of the stainless steel burner was 10 cm, and the flames were stabilized with a lip height of 10 mm. The heptane pool fire reached a steady state operating condition in approximately 3 to 4 minutes.

2.3. Experimental Arrangement

The near infrared fire detector was evaluated using both direct and reflected radiation. The location of the detector with respect to the fires for evaluation using direct and reflected radiation are shown in Figs. 2 and 3 respectively. For the experimental evaluation using direct radiation, the standard test fires were placed at a distance of 2 meters from the NIR fire detector.

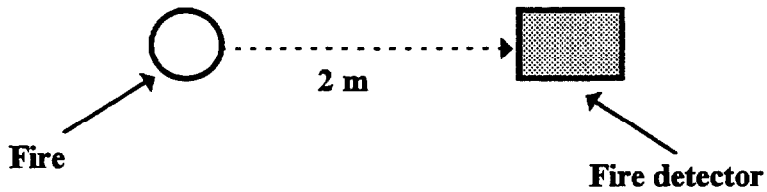

Figure 3. Experimental arrangement used for evaluation using direct radiation.

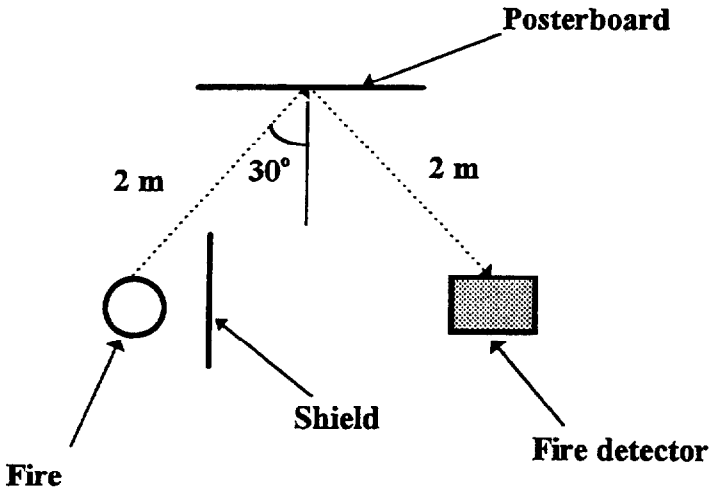

Figure 3. Experimental arrangement used for evaluation using reflected radiation.

For the experimental evaluation of the NIR fire detector utilizing reflected radiation, the direct radiation was blocked using a shield. The NIR fire detector and the test fires formed the two vertices of an equilateral triangle as shown in Fig. 3. The radiation from the fire was reflected onto the NIR fire detector using a poster board. The effect of different materials was briefly investigated using a brick wall, and a window pane at the same location of the poster board. These results are also presented in the following.

2.4. Results of the Experimental Evaluation

The results of the experimental evaluation are provided separately for the three open fires (TF1, TF4 and TF5) and the two smoldering fires (TF2 and TF3). The last fire (TF6) is an non-luminous alcohol fire and cannot be detected by the present NIR fire detector.

The probability density functions (PDFs) of spectral radiation intensity at 900 nm emanating from the open fires as measured by the NIR infrared detector are shown in Fig. 4. The PDFs of spectral radiation intensity incident on the fire detector when the fires were in its direct and indirect view are shown in the top and bottom panels of Fig. 4. When the open fires were in the direct view of the detector, the spectral radiation intensities incident on the detector ranged from a mean value of 100 W/m^2-μm-str. for the polyurethane foam to 300 W/m^2-μm-str. for the heptane pool. When the fire detector is not in the direct view of the fires, the only radiation incident on it was that reflected by the poster board. The poster board has very low reflectivity. Therefore, the spectral radiation intensities incident on the fire detector were approximately 40 to 50 times lower than those obtained from direct radiation. In addition, the open polyurethane foam and wooden crib fires were transient in nature. This causes the actual intensities measured by the detector to vary depending on the time lag before the measurement and the initiation of the fire. Therefore, the fire detection algorithm used in radiation detectors has to account for this widely varying magnitude in actual radiation intensities incident on it, without causing any false alarm.

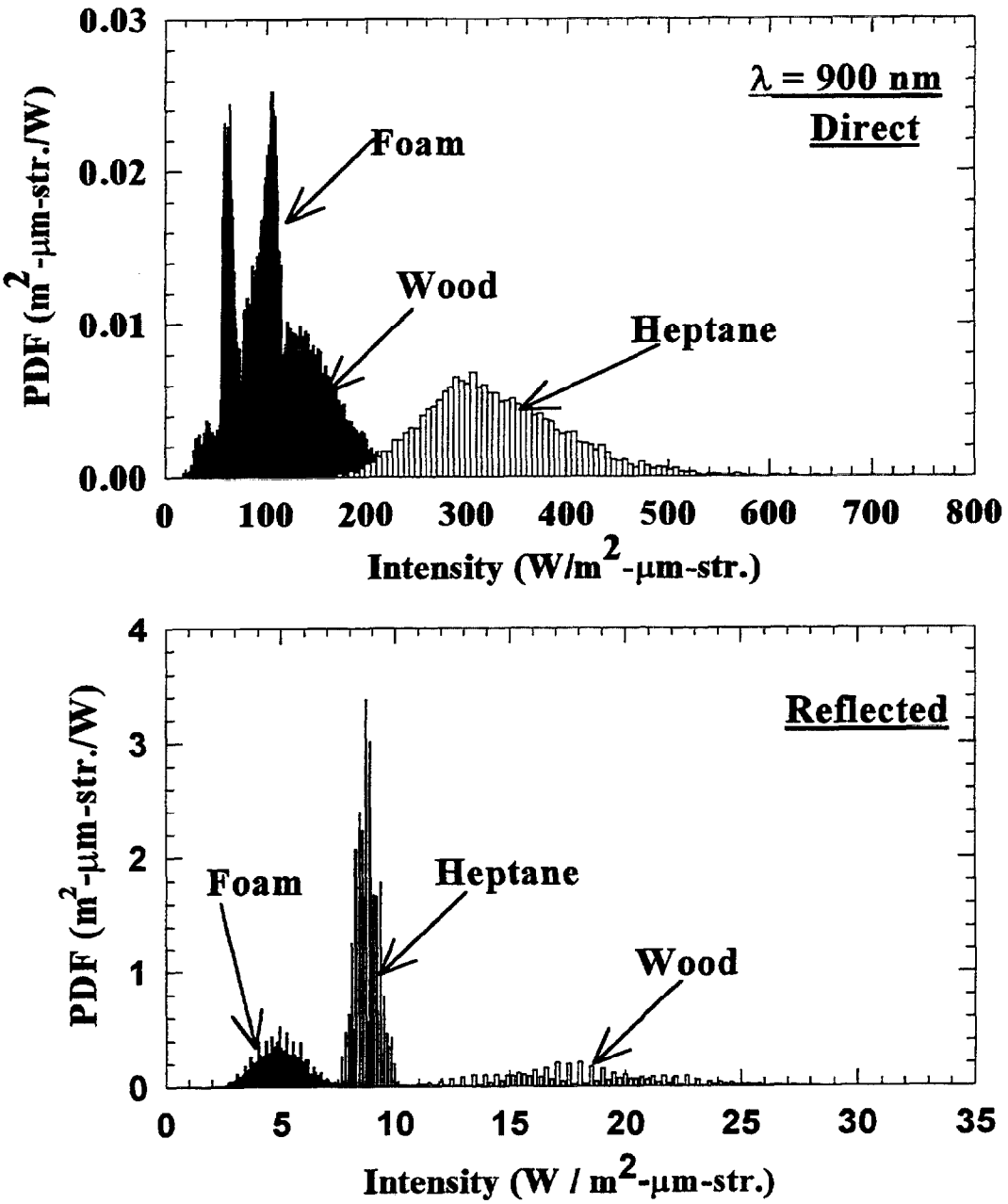

Figure 4. PDFs of spectral radiation intensities from the open fires.

The PDFs of spectral radiation intensity at 900 nm emanating from the smoldering fires are shown in Fig. 5. When the smoldering cotton fire is in the direct view of the detector, the spectral radiation intensities incident on the detector ranged from a 0.25 to 0.5 W/m^2-μm-str. The

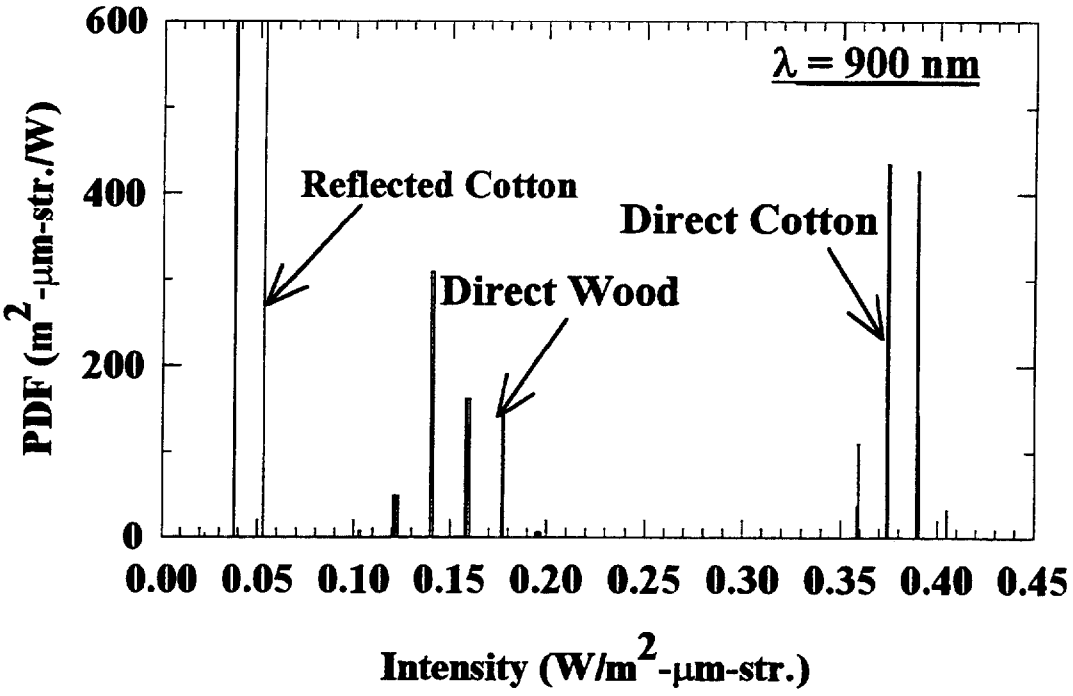

Figure 5. PDFs of spectral radiation intensities from the smoldering fires.

spectral radiation intensities from the smoldering wood fires were even lower, ranging from 0.1 to 0.18 W/m^2-μm-str. Similar to the open fires, the intensities obtained from reflected radiation were much lower than those obtained from direct radiation for the smoldering fires. The spectral radiation intensities from reflected radiation for the smoldering wood fire were below the detection limit of the NIR fire detector.

The major observation to be noted from the PDFs of spectral radiation intensities shown in Figs. 4 and 5 is that the magnitude of intensities incident on the detector can vary by approximately 5 orders of magnitude. Therefore, a fire detection algorithm based on the magnitude of intensities will either miss some of the fires (if the sensitivity of the detector is low) or suffer from false alarms from environmental radiation (for high sensitivity detectors).

The probability density functions (PDFs) of apparent source temperatures estimated from measurements of direct and reflected spectral radiation intensities at 900 and 1000 nm are shown in Fig. 6. The PDFs of apparent source temperatures obtained with the three open fires (heptane, foam and wood) in the direct view of the detector are shown in the bottom panel of Fig. 6. The apparent source temperatures for the three open fires ranged from 1300 to 1800 K.

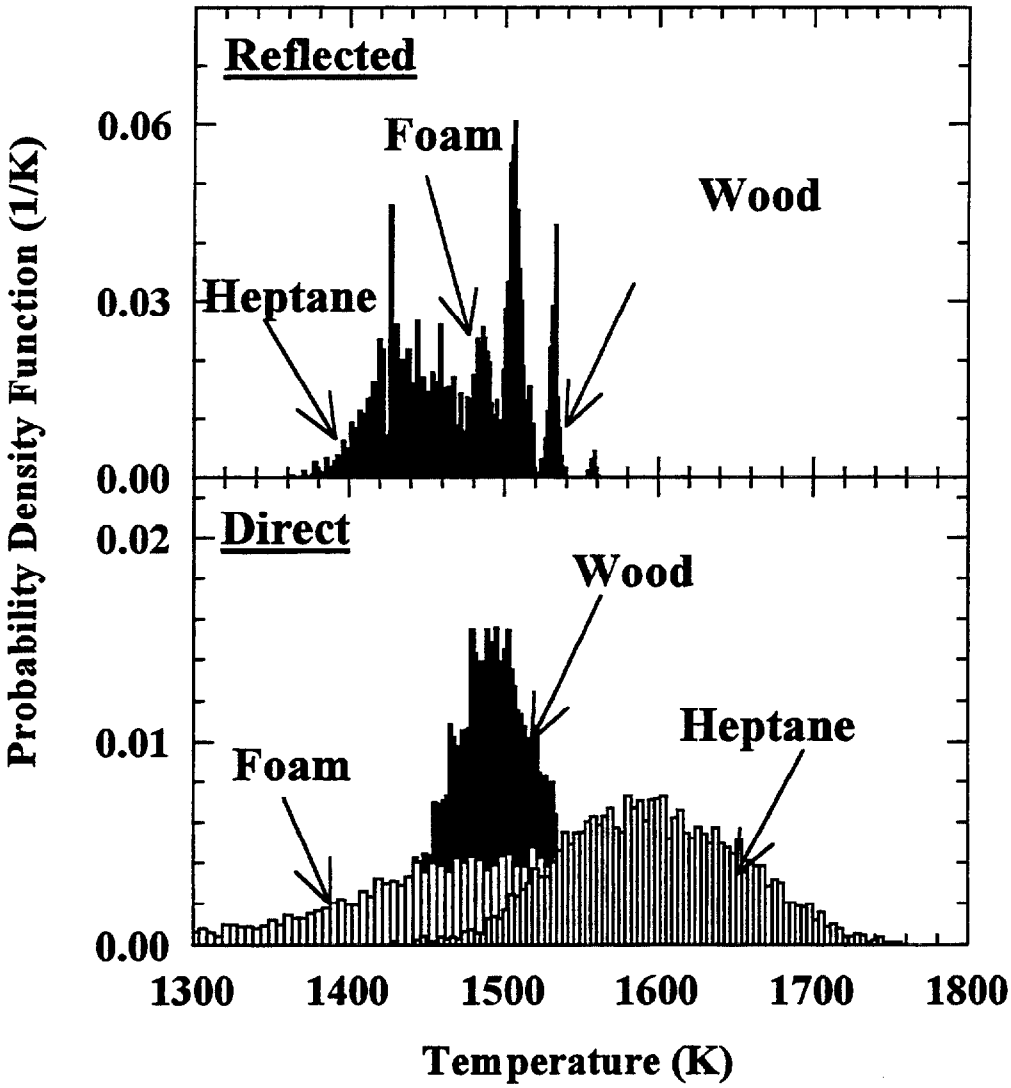

Figure 6. The PDFs of apparent source temperatures for the open fires.

The PDFs of apparent source temperatures for the three open fires when only reflected radiation was incident on the detector are shown in the top panel of Fig. 6. For liquid pool fires, the highest temperatures are usually associated with very low soot volume fractions, resulting in comparatively lower spectral radiation intensities. In addition, at the lowest temperatures, the spectral radiation intensities are very low due to the exponential nature of the Planck Function. Therefore, after one reflection, only the middle range of temperatures (with some spectral biasing) are detected by the NIR fire detector.

For the wooden crib and polyurethane foam fires, information on the correlation between local intensities and temperatures is not available. Therefore, the changes in the shape of the apparent source temperature PDFs could be due to a combination of factors, including spectral biasing of the reflected intensities, shape of the flame, and correlation between local temperatures and emissivities. In addition, these fire were transient in nature, and the temperatures obtained from direct and reflected radiation could be at different stages in the development of the fire. Despite the differences in the PDFs obtained from the direct and indirect viewing of the fire, all of the temperatures fall within 1000 to 2000 K.

The PDFs of apparent source temperatures estimated by the NIR fire detector for the smoldering fires (cotton fiber and wooden pellets) are shown in Fig. 7. Smoldering fires have much lower temperatures than open fires. The PDFs of apparent source temperatures obtained from direct radiation for the smoldering cotton fire varied from 900 to 1100 K, and that for the smoldering wood fire varied from 700 to900 K, as shown in the bottom panel of Fig. 7.

The PDF of apparent source temperatures estimated by the NIR fire detector using reflected radiation from the smoldering cotton fire was approximately 200 K lower. In addition, the PDF was not continuous. This is because the reflected intensities incident on the NIR fire detector from the smoldering cotton fire were very low. Therefore, the discretization error of the A/D converter became a significant factor in the apparent source temperatures estimated by the NIR fire detector. For the smoldering wood fire, the reflected intensities were below the detection threshold of the NIR fire detector.

Based on the PDFs of apparent source temperatures estimated by the NIR fire detector from the open and smoldering fires, one criteria for the existence of the fire in the vicinity of the detector can be identified. This criteria is that at least 40% of the apparent source temperatures estimated by the NIR fire detector should be between 600 and 2500 K. This is admittedly a very broad range of apparent source temperatures. However, there are very few sources of environmental radiation that would have an apparent source temperature that is within this range. For instance, solar radiation would yield an apparent source temperature of 6000 K. Two common source that could have apparent source temperatures between 600 and 2500 K are commercial hot plates and incandescent bulbs. Therefore, using only the PDF of apparent source temperatures as a fire detection algorithm would result in false alarms in the presence of a hot plate or an incandescent bulb.

The second characteristics of natural fires that can be used to eliminate these sources of false alarms is the power spectral density of spectral radiation intensities. The power spectral density of spectral radiation intensities emanating from natural fires have a very well defined low frequency component, and this can be exploited in fire detection algorithms.

The normalized power spectral densities (PSDs) of spectral radiation intensities at 1000 nm for the three open fires are shown in Fig. 8. For a unsteady signal $I_\lambda(t)$ being sampled at a frequency of M Hz, the normalized PSD E_N at a frequency f, is defined as:

$$E_N(f) = \frac{\int_0^f E(f)df}{\int_0^f S(f)df} \qquad (2.3)$$

where E(f) is spectrum function for the signal I_λ (t), divided by the mean square deviation of I_λ.

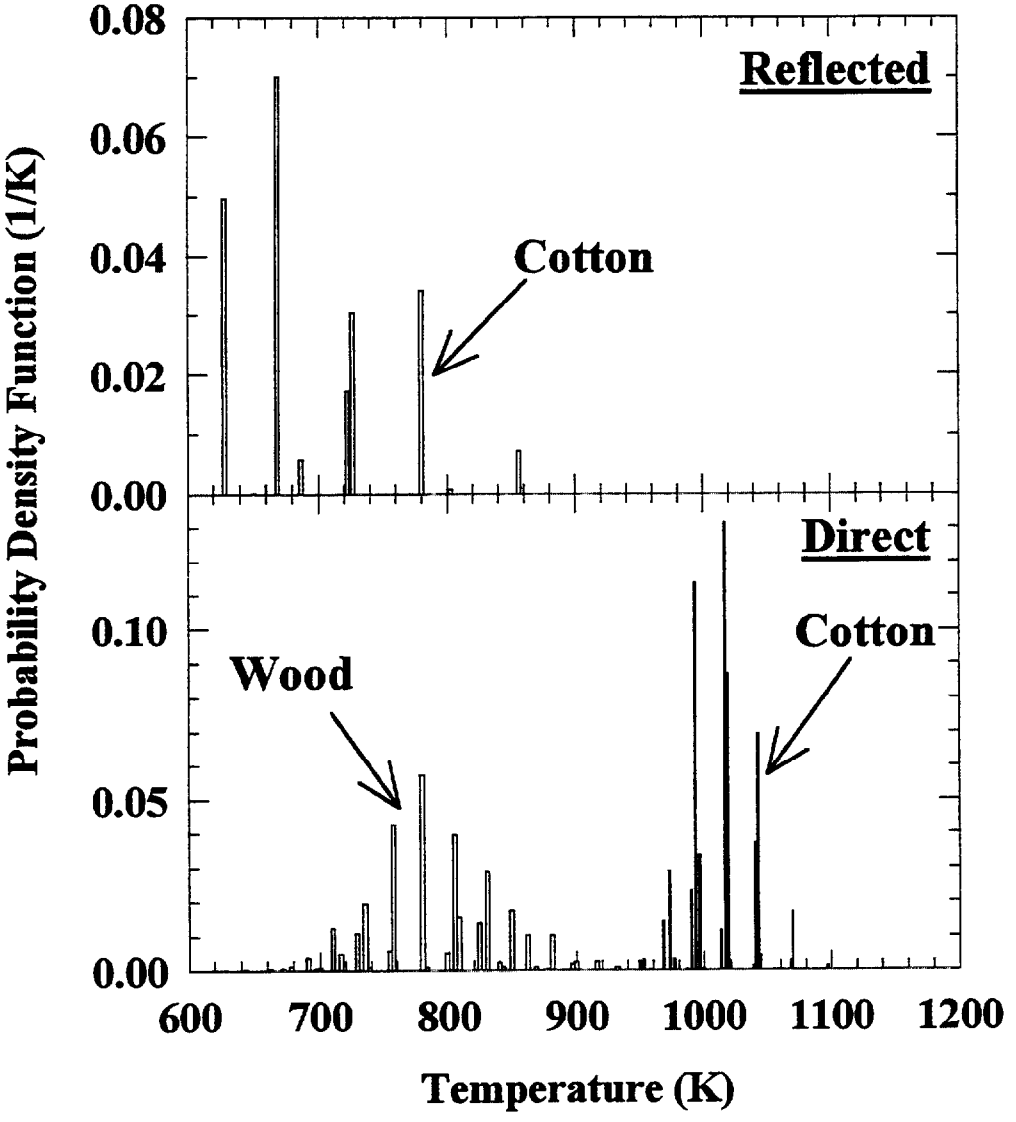

Figure 7. PDFs of apparent source temperatures for smoldering fires.

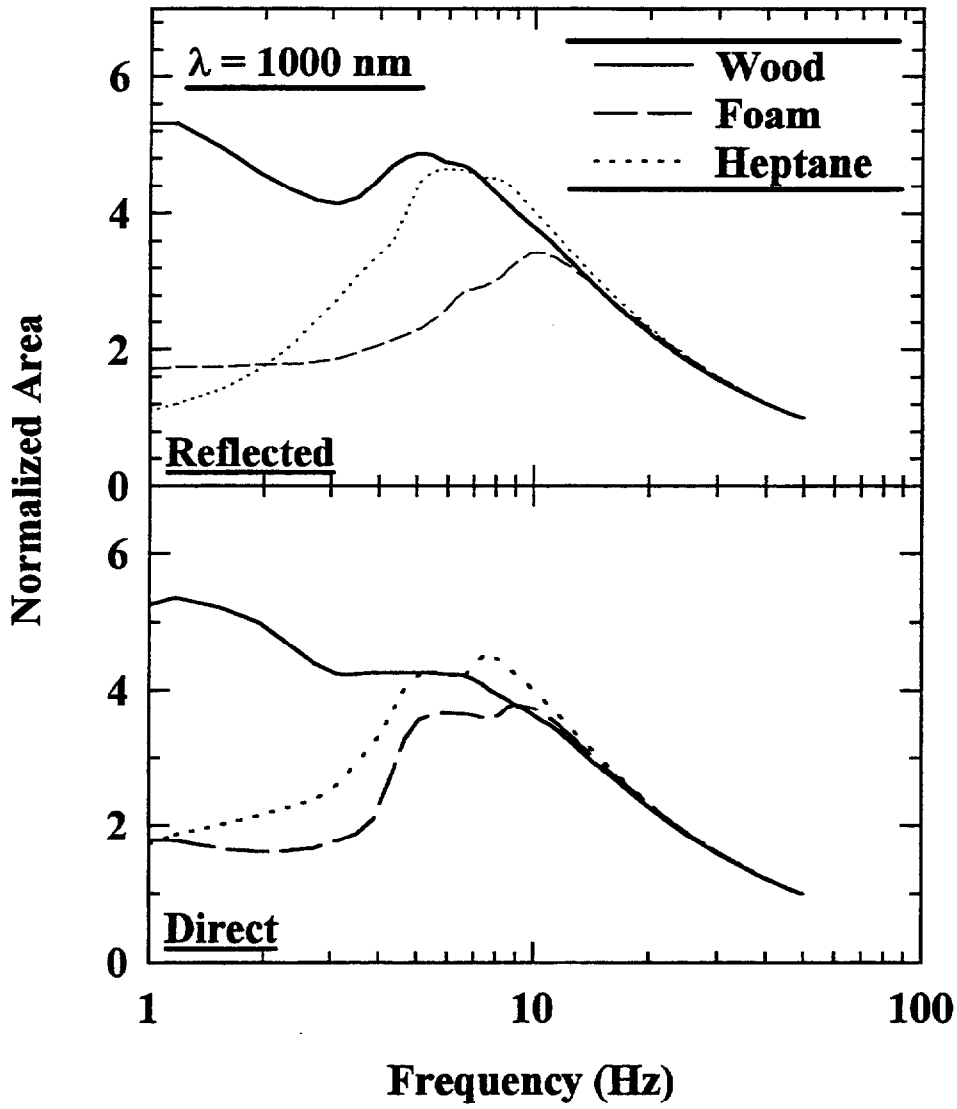

Figure 8. The normalized PSDs of spectral radiation intensities for the open fires.

The spectrum function is the Fourier transform of the auto-correlation coefficient, R(T) and is given by:

$$E(f) = 2\int_{-\infty}^{+\infty} R(t)\cos 2\pi ft\,dt \qquad (2.4)$$

S(f) is the spectrum function for white noise, which when sampled at a frequency of M (and low pass filtered at M/2), has a uniform value 2/M between 0 and M/2, and is 0 at other frequencies.

Physically, the normalized PSD at any frequency represents the ratio of the total energy of the signal below that frequency in comparison with a white noise source sampled with the same temporal resolution. The normalized PSDs shown in Fig. 8 imply that the total energy content of the spectral radiation intensity incident on the detector below a frequency of 10 Hz for all the three open fires is approximately four time higher than that of white noise for direct radiation. For reflected radiation, since the absolute values of the intensities are lower, the signal to noise ratio is lower. Therefore, the normalized PSD at 10 Hz is only about a factor of 3 higher than that of white noise.

The normalized PSDs of spectral radiation intensities at 1000 nm for the two smoldering fires are shown in Fig. 9. The intensities obtained from the direct view of the smoldering wood

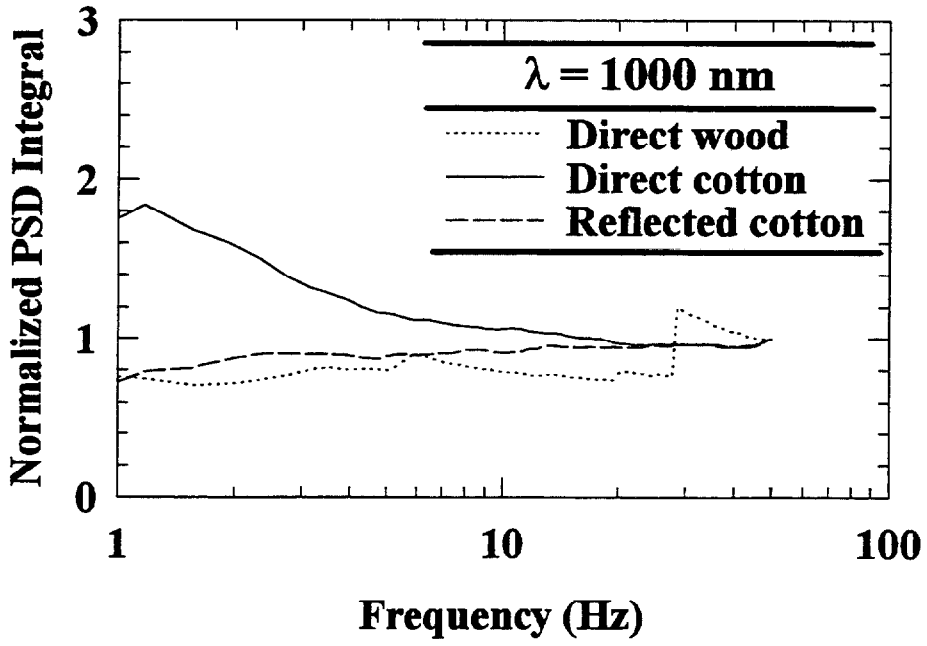

Figure 9. The normalized PSDs of spectral radiation intensity for the smoldering fires.

fire and from the reflected view of the cotton fire are barely above the noise level, and therefore could not be identified by the near infrared fire detector as valid fire signals. The major reason for the very poor performance with the smoldering wood fire is that the smolder surface is face down on the burner and therefore very little of the smoldering surface is visible. The standard test fire (TF3) is specifically designed to test smoke detectors and not flame detectors. For flame

detection, an alternative standard test for smoldering wood would be more appropriate. The smoldering cotton fire can be discriminated utilizing a A/D converter with a higher (16 bit) dynamic range.

Based on the above results, the second criteria for the existence of the fire near the vicinity of the NIR fire detector was established. The second criteria is that the normalized PSD of the spectral radiation intensity at 10 Hz should be at least 1.5 time greater than that obtained from white noise. This along with the first criteria (the 40% of the apparent source temperature should be between 600 and 2500 K) forms the basis of the fire detection algorithm of a NIR fire detector.

The effect of different building materials on the bias in the temperature estimated by the NIR fire detector was checked by using a propane flame, and viewing the reflections using a window pane and a brick wall. The PDFs of temperature obtained from radiation reflected off the window pane and the brick wall is shown in Fig. 10. There is a potential for approximately a 200 K upward bias in the temperatures estimated by a NIR fire detector. However, this still is well within the temperature range specified by criteria 1, confirming the utility of the NIR fire detector for monitoring multiple room enclosures.

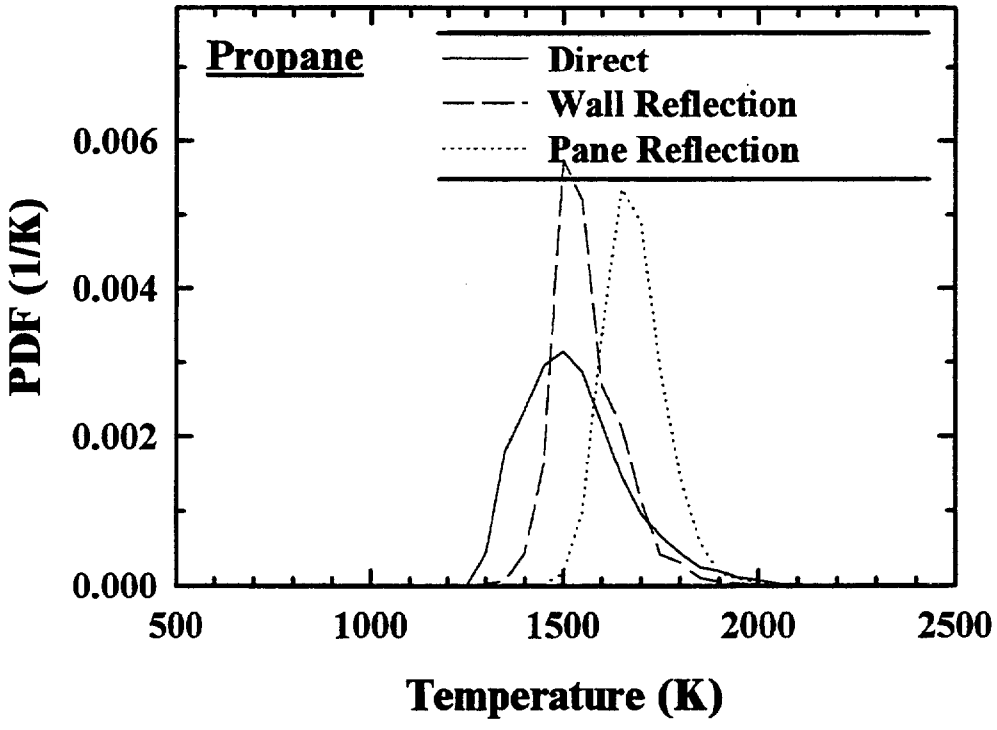

Figure 10. Effect of building materials on the apparent source temperatures.

The final part of the project converted the data acquisition and reduction program to enable the NIR fire detector to be used continuous monitoring. For continuously monitoring the environment for fire, data is collected for 25.6 seconds at 100 Hz providing 2560 intensity measurements at 900 and 1000 nm. From these intensity measurements a time series consisting of 2560 apparent source temperatures were calculated and used to obtain the PDF and the average normalized PSD (from 20 digital transforms of 128 points). The data reduction program takes approximately 10 seconds on the laboratory computer. If the two criteria for the existence of a fire in the vicinity of the NIR fire detector was satisfied, an alarm was sounded. The three open test fires were lighted at different times during the data collection cycle, and the number of cycles required for the alarm to be activated was noted. This provides a rough estimate of the response time of the detector in units of cycle time and is shown in Table 1.

Table 1: Response time for the NIR fire detector.

Fuel	Ignition time	Mode	E_N at 10 Hz	Cycles needed for alarm
Heptane	5	Direct	4.22	1
Heptane	10	Direct	4.19	1
Heptane	15	Direct	4.14	1
Heptane	20	Direct	4.24	2
Heptane	5	Reflected	3.54	1
Heptane	10	Reflected	3.67	1
Heptane	15	Reflected	3.75	1
Heptane	20	Reflected	3.97	2
Foam	5	Direct	3.13	1
Foam	10	Direct	3.03	1
Foam	15	Direct	3.62	2
Foam	20	Direct	3.55	2
Foam	5	Reflected	2.38	2
Foam	10	Reflected	1.88	2
Foam	15	Reflected	1.74	2
Foam	20	Reflected	1.58	2
Wood	NA	Direct (1)	2.06	5
Wood	NA	Direct (2)	1.83	7
Wood	NA	Reflected (1)	1.78	7
Wood	NA	Reflected (2)	2.03	10

The open heptane and foam fires were typically detected very quickly within one or two data collection cycles (35 to 70 seconds) after ignition from both direct and reflected radiation. In addition, for almost all cases, the normalized PSD at 10 Hz was very distinct from white noise Discrimination by PDF is always successful as soon as the fire is started, since the temperatures are very easily obtained. However, for the open wood fires, the fires had to reach a dimension of approximately 3 inches (for direct radiation) and 8 inches (for reflected radiation) before the normalized PSD was 1.5 times greater than that obtained from white noise. In addition, no instances of false alarms were ever recorded during the entire operation over a two month period.

3. Numerical Evaluation

3.1. DPF Formulation

The primary objective of the numerical evaluation is to develop a methodology to calculate the intensities incident on a fire detector from a source within an enclosure. The anticipated benefit of the evaluation is to provide a design tool to help fire safety engineers determine the optimum location of a NIR fire detector for monitoring a multiple room enclosure. The spectral radiation intensities incident on the fire detector within an enclosure were obtained using a ray tracing algorithm in conjunction with the DPF method. The basic numerical method was evaluated for two simple geometries (a cylindrical and a rectangular enclosure) during the present grant period.

The first problem studied by the simulations was to determine the effect of the reflected radiation on the apparent source temperatures inferred by the NIR fire detector. For this purpose, a constant temperature source was placed at one end of a cylindrical enclosure as shown in Fig. 11 (surface A_1) and the detector was placed on the other end (surface A_2). The cylindrical walls

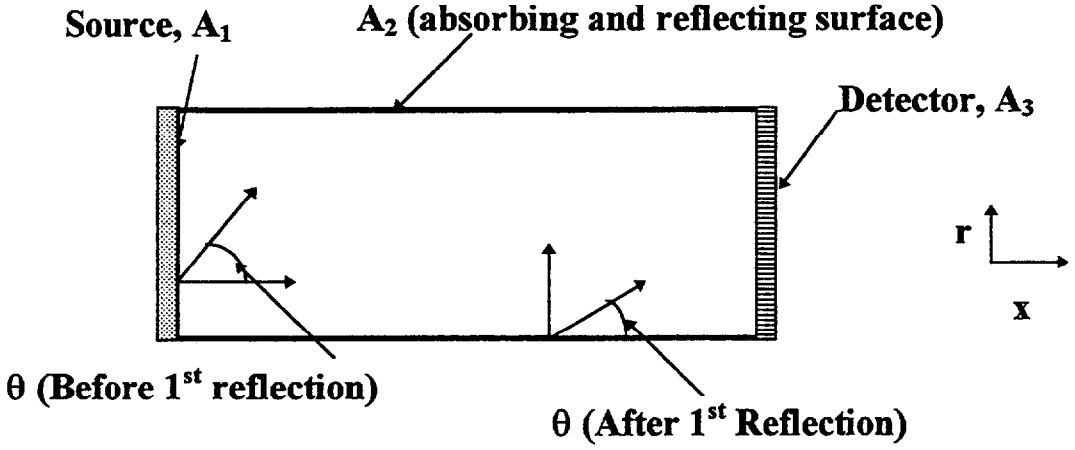

Figure 11. Cylindrical enclosure used to simulate the effect of reflections.

of the enclosure was assumed to absorb and reflect (specularly and diffusely) the radiation incident on it. The spectral absorptivity and reflectivity of the cylindrical walls, in addition to the aspect (length to diameter) ratio of the enclosure, were the parameters of the simulation.

The source emits photons in all angles and wavelengths. The number of photons emitted in a particular angle and wavelength depends on the directional and spectral emissivity of the source. The cylindrical surface of the enclosure, of length L and radius R, absorbs some of the photons incident on it and reflects the rest both specularly and diffusely. The trajectories of the photons emitted by the source and reaching the NIR fire detector were followed using the DPF method. The spectral radiation intensity (i_λ) incident on the detector at two wavelengths (λ_1 and λ_2) were calculated and used to estimate the source temperature as:

$$T = \frac{hc}{k}\left(\frac{1}{\lambda_1} - \frac{1}{\lambda_2}\right) / \ln\left\{\left(\frac{\varepsilon_{\lambda 2}\lambda_2^5}{\varepsilon_{\lambda 1}\lambda_1^5}\right)\left(\frac{I_{\lambda 2}}{I_{\lambda 1}}\right)\right\} \tag{3.1}$$

where C_2 is the second radiation constant and ε_λ is the spectral emissivity. A temperature of 1500 K and spectral emissivity values of 0.111 and 0.10 for the 900 and 1000 nm wavelengths were chosen for source. These values yield emission intensities from the hot surface that are representative of the average intensities leaving luminous flames (Sivathanu et al., 1991).

The surfaces and angles shown in Fig. 11 are discretized to obtain surface and angular ranges, similar to the method of Billings et al. (1991). The source surface A_1 is divided into N surface ranges, which are of the shape of circular rings with equal width Δr each. The polar angle θ, and the azimuthal angle ϕ, are divided into N equal angle ranges, $\Delta\theta$ and $\Delta\phi$ respectively.

The normalized probability density function (PDF) of a photon leaving surface A_1 at a radius r, and polar and azimuthal angles θ and ϕ is given by (Sivathanu and Gore, 1994):

$$f(r,\mu,\phi) = f(r)f(\mu)f(\phi) \tag{3.2}$$

$$f(r) = 2r / R^2 \tag{3.3}$$

$$f(\mu) = 2\mu \tag{3.4}$$

$$f(\phi) = 1/2\pi \tag{3.5}$$

where μ is equal to cos θ and R is the radius of the cylinder. Eqs. (3.2-3.5) represent Lambertian emission from the surface A_1. Following Sivathanu and Gore (1993), the three PDFs associated with the emission of the photons from surface A_1 are discretized to obtain their respective DPFs P(r), P(μ), and P(ϕ) as:

$$P(r) = (r_i; P_{ri}); i = 1,N \tag{3.6}$$

$$P(\mu) = (\mu_j; P_{\mu j}); j = 1,N \tag{3.7}$$

$$P(\phi) = (\phi_k; P_{\phi k}); k = 1,N \tag{3.8}$$

where

$$P_{\Phi i} = \int_{\Phi_i - \Delta\Phi/2}^{\Phi_i + \Delta\Phi/2} f(\Phi)d\Phi \tag{3.9}$$

Φ represents one of the three variables r, μ, or ϕ and P_{ri}, $P_{\mu j}$ and $P_{\phi k}$ are the probabilities that a photon is emitted from the surface range r_i, polar angular range θ_j and azimuthal angular range ϕ_k.

The photon emitted from r_i, θ_j, ϕ_k intersects the cylinder at an x-location (x^1):

$$x^1 = \frac{l_j\left[r_i m_{jk} + \{R^2(m_{jk}^2 + n_{jk}^2) - r_i^2 n_{jk}^2\}^{1/2}\right]}{m_{jk}^2 + n_{jk}^2} \tag{3.10}$$

where the superscript 1 represents the first interaction of the photon with the cylindrical surface and l_j, m_{jk} and n_{jk} are the direction cosines given by:

$$l_j = \text{Cos } \theta_j; m_{jk} = \text{Sin } \theta_j \text{Cos } \phi_k; n_{jk} = \text{Sin } \theta_j \text{Sin } \phi_k \tag{3.11}$$

If x^1_{ijk} is greater than the length of the tube, the photon strikes the detector. Else, it intersects the wall where it undergoes a diffuse or specular reflection. The photons which leaves surface A_1 and intersects with the wall, will be characterized by a location given by the surface range x_i^1 (which is on surface A_2), and new polar and azimuthal angles given by θ_j^1, and ϕ_k^1, determined by whether it is specularly or diffusely reflected. This is identical to the two state parameters in the Markov chain method of Billings et al. (1991) and x_i^1, θ_j^1, and ϕ_k^1 can be considered to be the new three parameter state of the photon. The point of departure from the Markov chain method is that each of these states have a probability associated with them through the DPF calculations, rather than the probability being associated with the transition of a photon from the old state of r_i, μ_j, and ϕ_k to the new state of x_i^1, μ_j^1, and ϕ_k^1.

The probabilities associated with the new location (x^1) of reflection treated as "re-emission" of the photon are formed from all possible combinations of the old states and can be expressed as (Sivathanu and Gore, 1994):

$$P(x^1) = (x_i^1; P_{x_i}^1); i = 1, N \tag{3.12}$$

where

$$P_{x_i}^1 = \sum_{i=1}^{N} \sum_{j=1}^{N} \sum_{k=1}^{N} \delta(x^1) P_{ri} P_{\mu j} P_{\phi k} \rho_\lambda \tag{3.13}$$

where $\delta(x^1) = 1$ if $x_i - \Delta x_i / 2 \le x^1 \le x_i + \Delta x_i / 2$; $\delta(x^1) = 0$ else, and x^1 is obtained from Eq. (3.10). Physically, Eqs. (3.10-3.13) imply that the probability of a photon starting from surface range x^1_i is the sum of all the products of the probabilities that the photon started from r_i, θ_j, and ϕ_k and intersected the curved surface between $x_i - \Delta x_i/2$ and $x_i + \Delta x_i/2$. The probability of each photon is multiplied by the spectral reflectivity (ρ_λ) since a certain percentage of these photons will be absorbed by the curved surface. Of the reflected a photons, a certain percentage is specularly reflected and the remainder is diffusely reflected. It is noted that for each value of i, j and k under the summation signs, the product $\delta(x^1) P_{ri} P_{\mu j} P_{\phi k} \rho_\lambda$ is identical to the transition probability of the photon going from states r_i, μ_j, and ϕ_k to the new state x^1_i after absorption by the surface.

It is slightly more difficult to calculate the probabilities for the angles of departure of the reflected photons, since these probabilities depend on the x-location. If the surface is totally diffuse (Sivathanu and Gore, 1994), then these probabilities are independent of the location x_i and are identical to the probabilities of Lambertian emission. However, for the present problem, the surface reflects specularly and diffusely, and therefore, we need a joint probability density function for the angles of emission and location of the photon after reflection. The method of calculating these joint probability density functions are in principle identical to those given in Eqs. (3.10-3.13). For the polar angle θ^1, and axial location x^1, the joint discrete probability function of re-emission, is defined as (Sivathanu and Gore, 1993):

$$P(\mu^1, x^1) = ((\mu_j^1, x_i^1); P^1_{\mu_j x_i}); j, i = 1, N \tag{3.14}$$

where $P^1_{\mu_j x_i}$ is the probability that a photon is emitted from the surface range x_i in the polar angle range θ_j after 1 interaction with the wall. For specular reflection the new polar angle of emission of the reflected photon which is incident at an angle of θ_j is given by:

$$\theta^1 = \theta_j \tag{3.15}$$

The probability associated with the photons re-emitted in the θ^1_j direction consists of both a specular component $P^{1s}_{\mu_j x_i}$ which is given by:

$$P^{1s}_{\mu_j x_i} = \sum_{i=1}^{N} \sum_{j=1}^{N} \sum_{k=1}^{N} \delta(x^1)\delta(\theta^1) P_{ri} P_{\mu j} P_{\phi k} \rho_\lambda \frac{\rho_{s\lambda}}{(\rho_{s\lambda} + \rho_{d\lambda})} \tag{3.16}$$

where $\delta(\theta^1) = 1$ if $\mu_j - \Delta\mu_j / 2 \le \text{Cos}\ (\theta^1) \le \mu_j + \Delta\mu_j / 2$, and $\delta(\theta^1) = 0$ else. The superscript 's' implies that only the spectral component has been used for calculating these probabilities. The last term in Eq. (3.16) represents the fraction of photons that undergoes specular reflection. The probability of the diffuse part is added to that of the specular component to obtain the joint discrete probability function of a photon emitted from the surface range x_i in the polar angle range θ_j after 1 interaction with the wall:

$$P^1_{\mu_j x_i} = P^{1s}_{\mu_j x_i} + 2.\mu_j * \Delta\mu_j (P^1_{x_i} - \sum_{j=1}^{N} P^{1s}_{\mu_j x_i}) \tag{3.17}$$

The second term in Eq. (3.17) distributes the probabilities associated with the diffuse component to the different θ_j direction based on Lambertian emission given by Eq. (3.4).

Finally, the joint DPF of axial location, polar and azimuthal angle $P^1_{\phi_k \mu_j x_i}$ after 1 interaction with the wall is calculated in a similar manner. For specular reflection, the azimuthal angle of emission ϕ^1 after one reflection, for a photon which was emitted from surface A_1 in the range ϕ_k is:

$$\phi^1 = \phi_k \tag{3.18}$$

and the associated probability is given by:

$$P^{1s}_{\phi_k \mu_j x_i} = \sum_{i=1}^{N} \sum_{j=1}^{N} \sum_{k=1}^{N} \delta(x^1)\delta(\theta^1)\delta(\phi^1) P_{ri} P_{\mu j} P_{\phi k} \rho_\lambda \frac{\rho_{s\lambda}}{(\rho_{s\lambda} + \rho_{d\lambda})} \tag{3.19}$$

where $\delta(\phi^1) = 1$ if $\phi_k - \Delta\phi_k / 2 \le \phi^1 \le \phi_k + \Delta\phi_k / 2$, and $\delta(\phi^1) = 0$ else. As before we add the probabilities associated with the diffuse component of reflection as:

$$P^1_{\phi_k \mu_j x_i} = P^{1s}_{\phi_k \mu_j x_i} + \frac{\Delta\phi}{2\pi}\left(P^1_{\mu_j x_i} - \sum_{k=1}^{N} P^1_{\phi_k \mu_j x_i}\right) \tag{3.20}$$

At the end of the above procedure, Eq. (3.20) represents the probability associated the photon emission from surface A_2 (see Fig. 11) in the surface range x_i, and angular range μ_j, and ϕ_k after one reflection. Summing up these probabilities for all the surface and angular ranges yields the total probability that a photon initially emitted from surface A_1 will interact with the surface A_2. The remaining probabilities represent the view factor (Sivathanu and Gore, 1994) from the hot end of the cylinder to the cold end.

The next step in the process is to calculate the subsequent trajectories for the photons that have undergone one reflection with the wall. The radial location of the photons is no longer an independent variable, since all the photons now start from the wall with radius R, however their axial location varies from 0 to L. The photons are started from all the N bins of x_i^1, μ_j^1, and ϕ_k^1. The x coordinates of the second (and subsequent) intersections are given by:

$$x^2 = x_i^1 + 2l_j \{Rm_{jk} / (m_{jk}^2 + n_{jk}^2)\} \tag{3.21}$$

where the superscript '2' is a counter indicating the second interaction of the photon with the wall. The probabilities associated with each photon that undergoes this interaction are given by $P^1_{\phi_k \mu_j x_i}$. These probabilities are rebinned using the procedure explained in Eqs. (3.13,3.17, and 3.20) to obtain $P^2_{\phi_k \mu_j x_i}$. The solution procedure is carried forward to obtain $P^3_{\phi_k \mu_j x_i}$,

$P^4_{\phi_k \mu_j x_i}$, ... The process is terminated once more than 99.5% of the photons have been absorbed by the cylindrical surface or leave the enclosure through the right and left ends.

The simulations to calculate the intensity incident on the detector were carried out with 50 ranges of polar and azimuthal angles and 50 surface ranges. For the Markov chain method, for even one interaction (e.g. the n-1 to the n^{th} interaction) the transition probability matrix would have 50x50x50 elements, with each element containing the probability of transition from x^{n-1}_i, θ^{n-1}_j, ϕ^{n-1}_k to x^n_i, θ^n_j, ϕ^n_k. These probabilities are difficult to compute when n is greater than 2 for such a large number of surface and angular ranges. In the DPF method, the probabilities associated with each interaction Eqs. (3.13, 3.17, and 3.20) were obtained by tracking a total of 125000 photon through just one interaction with the wall. It is noted that the recursive nature of the algorithm results in a computational advantage over explicit solutions, since the probabilities are always rebinned after one interaction with the wall, thereby restricting the total number of trajectory calculation to always 125000, despite the specular/diffuse nature of the interaction and the three-dimensional trajectory. In addition, all possible photon trajectories (resolved to the surface and angular ranges) which have a probability of greater than 1 in 1000 are computed. This feature provides solutions with a high degree of accuracy.

The disadvantage over the Markov chain method is that since the transition probabilities are not explicitly stored, any surface property changes will require the simulation to be repeated. However, if only the temperature of the source is changed, the probabilities can be explicitly used to find the intensity incident on the detector.

The geometry used for the simulations in a rectangular enclosure is similar to that described for the axisymmetric enclosure. The rectangular enclosure of length L, width and height a, has an high temperature source (fire) at one end, and a detector at the other end as shown in Fig. 12. Part of the radiation emitted by the source is absorbed by the walls of the enclosure, and the remainder reflected both diffusely and specularly.

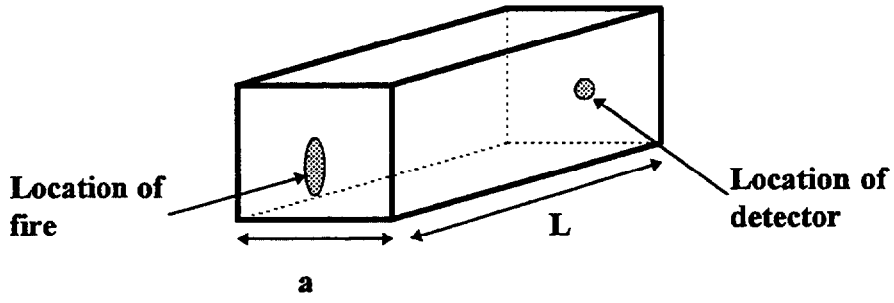

Figure 12. Rectangular enclosure used to simulate the effect of reflections.

To simulate a fire source at one end, the angular distribution of spectral radiation intensity leaving the fire is needed. This was obtained experimentally as described in the next section.

3.2. Description of Angular Measurements of Radiation Intensity

The spectral radiation intensities emanating from an heptane pool fire were measured at different polar angles using an optical fiber light guide as shown in Fig. 13. The objective of these

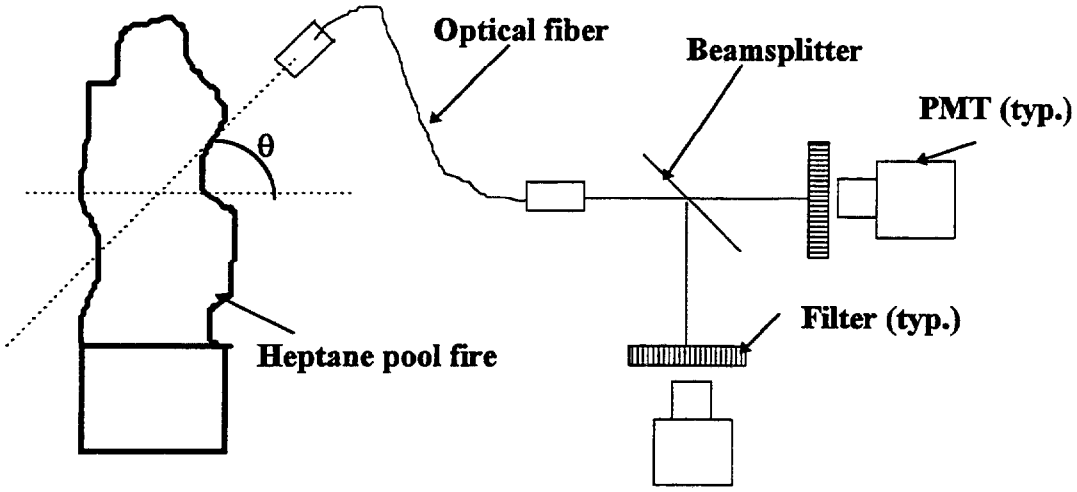

Figure 13. Experimental arrangement used for the angular measurements.

measurements was to obtain data to be used as input for the numerical simulations involving a test fire within an arbitrarily shaped enclosure. The measurements were obtained with a location on the axis at half the visible flame height as the reference point for the polar and azimuthal angles. The radiation emitted by the heptane pool fire was measured at 10 polar angles (θ from -60 to +60) using an optical fiber and two PMTs. The PMTs had optical filters centered at 900 and 1000 nm (half bandwidth of 10 nm) in front of them. The PMTs were calibrated using a blackbody and the joint PDFs of spectral radiation intensities at 900 and 1000 nm emanating from the fire for the different angles were obtained. The heptane pool fire is axisymmetric. Therefore, the radiation is uniform in the azimuthal direction.

A sample of the data obtained from the heptane pool fire is shown in Fig. 14. The variation in the mean and RMS of spectral radiation intensities with the polar angle is shown in the bottom panel of Fig. 14. As the polar angle either increases or decrease from horizontal, the mean spectral radiation intensities increase. This is a direct effect of the increase in the path length with either an increase or decrease of the polar angle from zero. There is no variation with azimuthal angle for the axisymmetric (in the time averaged sense) pool fire.

The variation of the mean apparent source temperatures with polar angle is shown in the top panel of Fig. 14. Despite the variation in mean spectral radiation intensities with the polar angle, the mean and RMS of apparent source temperatures are constant. This is to be expected since the temperatures estimated by the near infrared fire detector are always biased towards the highest values along the path.

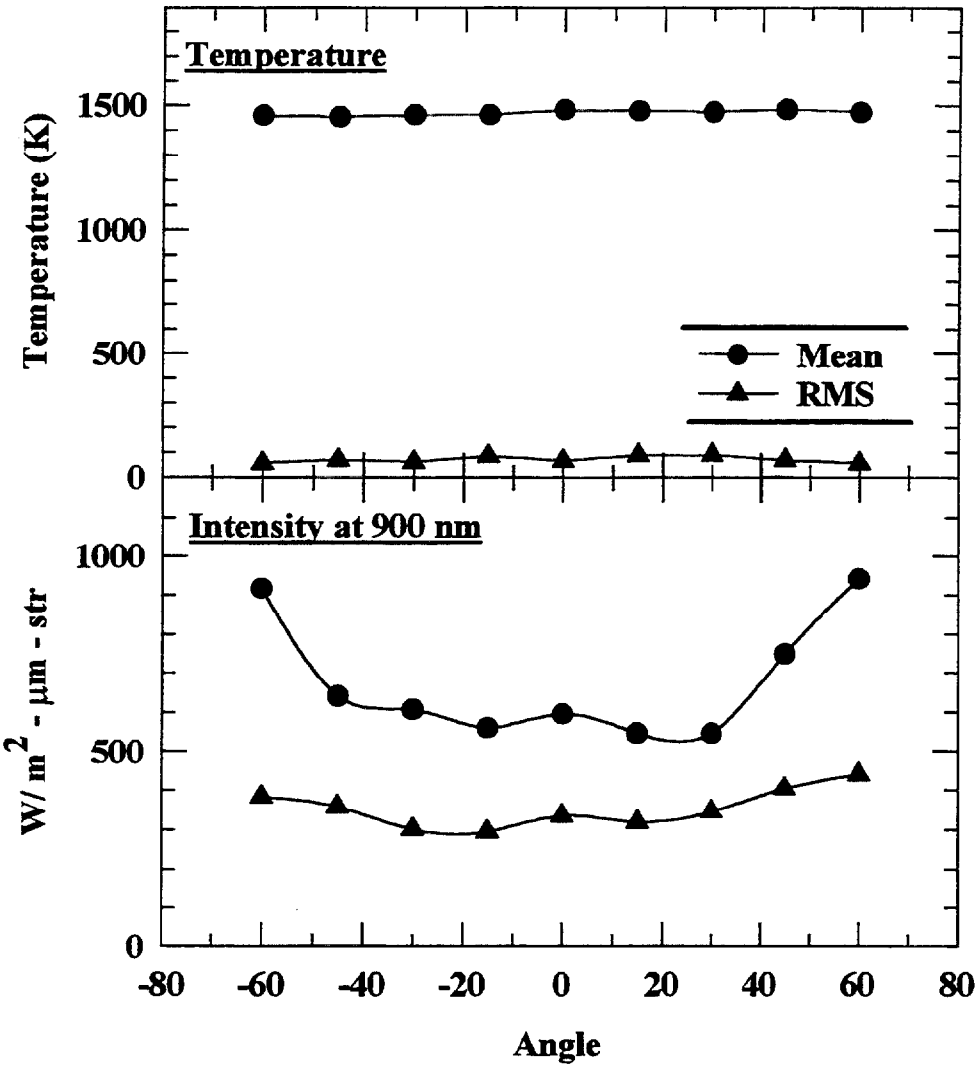

Figure 14. Variation of radiation properties with angle for an heptane pool fire.

The DPF simulations described above were extended to accommodate the data obtained from these angular measurements of spectral radiation intensities obtained from the heptane pool fire. The heptane pool fire was assumed to be located at the center of one end of the cylindrical or rectangular enclosure. The fire detector was located at the other end of the enclosure. The aspect ratio of the enclosure was fixed at 3. The walls of the enclosure were assumed to have a coating with reflectivity of 0.8 at 1000 nm and 0.88 at 900 nm. The specularity of the reflectivity was set at 0.4. The spectral radiation intensities obtained from the angular measurements were input into the program as joint probability density functions of spectral radiation intensities which varied with the polar angle, θ.

3.3. Results of the Numerical Simulations

The results of the simulations using a constant temperature source of 1500 K are presented first. The effect of the aspect ratio on the apparent source temperatures estimated by the NIR fire detector within a cylindrical enclosure is shown in Fig. 15. The walls of the

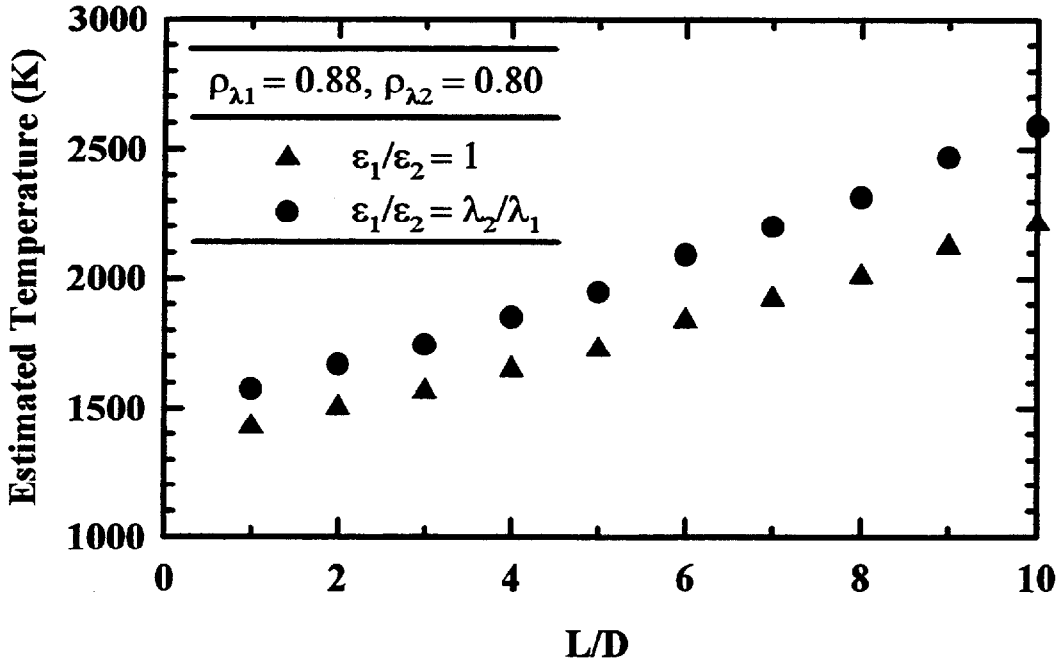

Figure 15. Estimated temperature variation with aspect ratio for a cylindrical enclosure.

enclosure were assumed to have an absorption coefficient which varied inversely with wavelength, typical of pigments used in commercial paints. When the aspect ratio is zero, the estimated temperature is 1500 K since only direct radiation is incident on the detector. The absorptivity of the paint was assumed to be 20% at 1000 nm.. As the aspect ratio of the cylindrical enclosure increases, the radiation incident on the detector consists of photons that have undergone multiple reflections with the walls of the enclosure. Therefore, the longer wavelength radiation is preferentially absorbed, leading to higher estimates for the apparent source temperatures. At an aspect ratio of 5, more that 70% of the photons have undergone at least 5 or more interactions with the wall coating, and the measured source temperature is higher by approximately 500 K than the actual value.

The effect of the specularity of reflectivity on the estimated temperatures is shown in Fig. 16 for a cylindrical enclosure with an aspect ratio of 3. The effect of reflectivity depends on the number of interactions the photons undergo with at the wall. An increase in the degree of

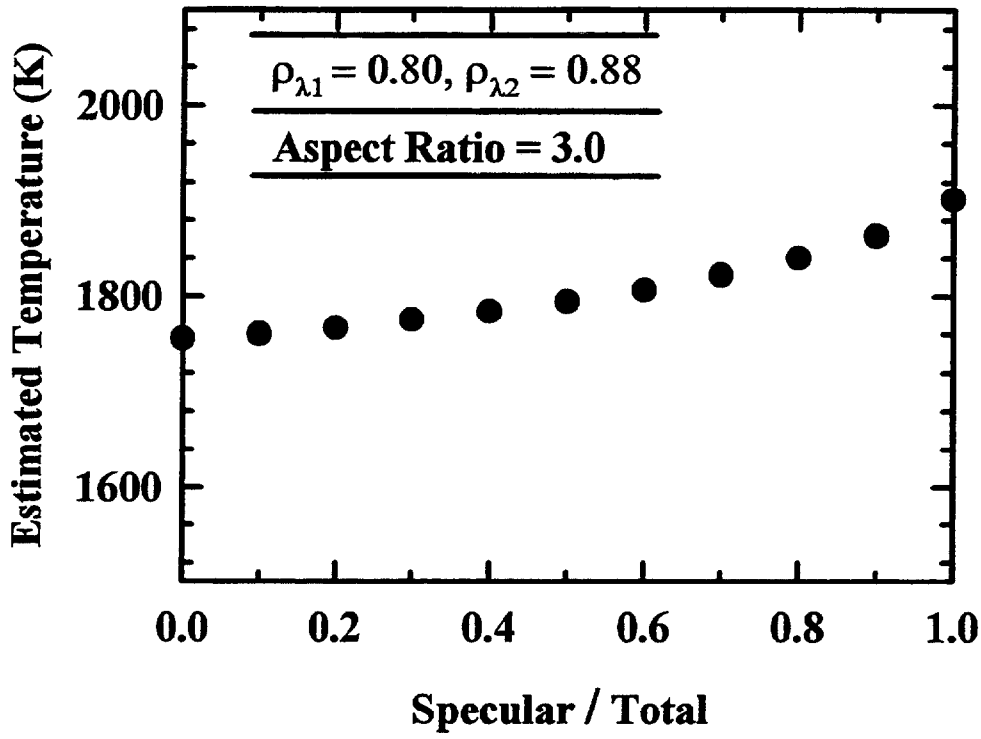

Figure 16. Estimated temperature variation with specularity for a cylindrical enclosure.

specularity increases the number of photons that reach the detector after an interaction with the wall. Therefore, the temperatures estimated by the detector are biased upwards since this larger fraction of the photons have undergone preferential longer wavelength absorption. When the specular reflection is unity, approximately 85% of the radiation incident on the detector is from photons that have undergone multiple reflections at the wall.

The variation in the measured source temperatures with reflectivity of the cylindrical surface is shown in Fig. 17. The ratio of specular to total reflectivity of the surface was set at 0.4. As the reflectivity of the cylindrical surface is decreased, a larger fraction of the photons is absorbed at the cylindrical surface and a higher percentage of the radiation incident on the detector is from direct radiation, leading to a better estimate of the source temperature.

The variation in estimated temperature with specularity of the reflectivity for a rectangular enclosure is shown in Fig. 18. The calculations were repeated using a Monte Carlo simulation with the same number of photons as in the DPF method . The accuracy of the DPF method over the Monte Carlo simulations for the same number photons is evident from Fig. 18. For highly

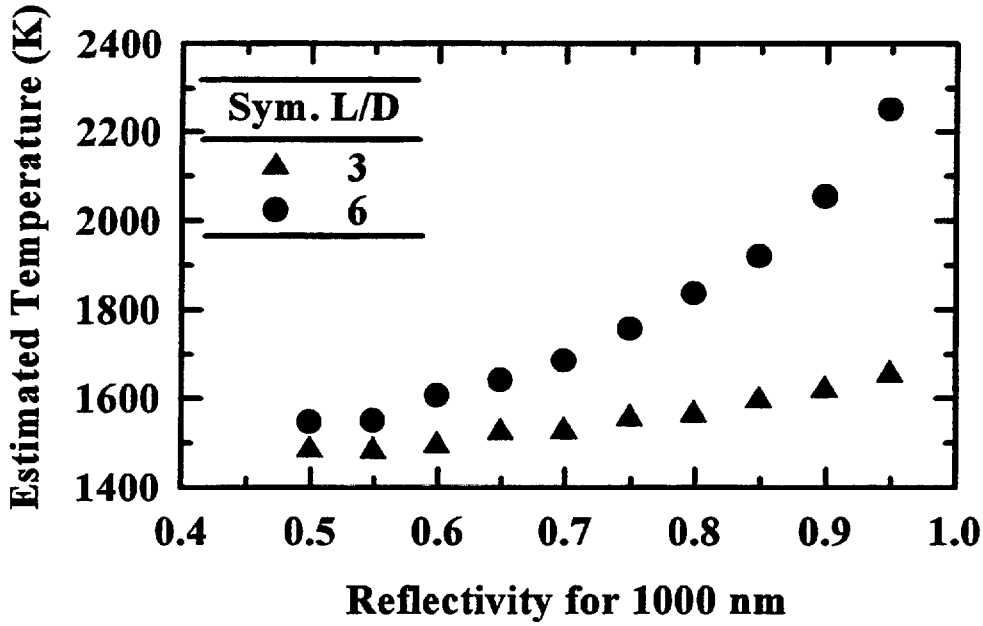

Figure 17. Estimated temperature variation with reflectivity for a cylindrical enclosure.

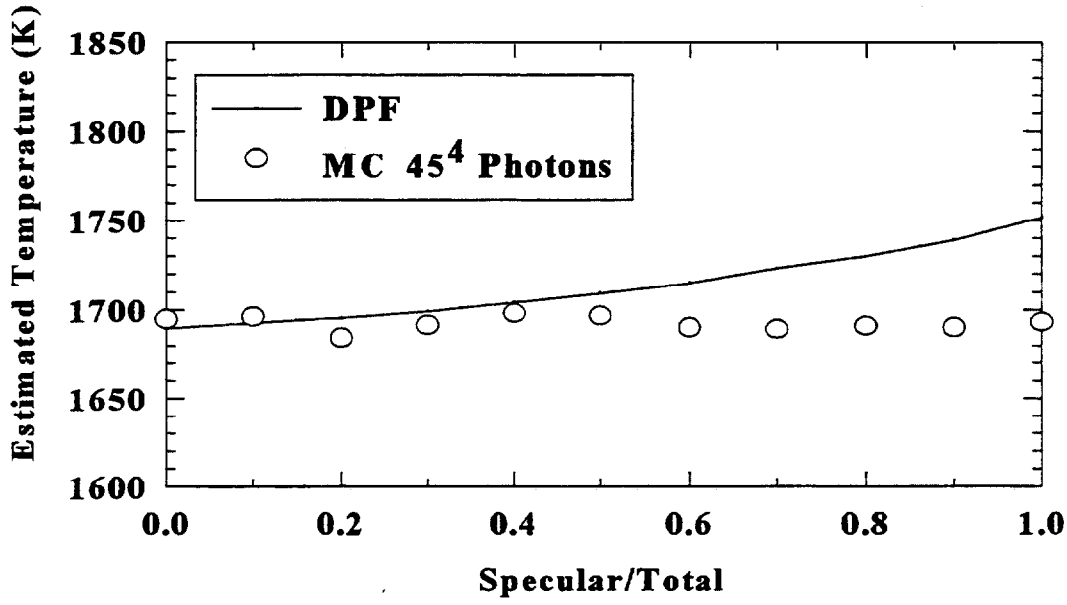

Figure 18. Estimated temperature variation with specularity for a rectangular enclosure.

specular surfaces, the effect of the reflected photons on the estimated source temperatures is not captured adequately by the Monte Carlo method. For highly specular surfaces, a larger fraction of the photons incident on the detector has undergone multiple interactions with the wall, and adequate statistical sampling of these reflected photons (Sivathanu and Gore (1994))becomes an important issue. The Monte Carlo results would improve if a larger number of photons was initiated from the source.

Unfortunately, there are no analytical solutions available that can be compared with the numerical results discussed above. However validation of the code was achieved by examining some specific conditions for which analytical solutions are available. When the reflectivity of the cylindrical walls was set to zero or 1 for both wavelengths, the temperature inferred by the simulation was 1500. In addition, when the reflectivity was set to zero, the normalized intensity incident on the detector was within 0.01 % of the geometrical view factor.

3.4 Results of Fire Detection Simulations

Having validated the numerical code to a limited extent, the constant temperature source was replaced with the experimental data discussed in the previous section to simulate an heptane pool fire within cylindrical and rectangular enclosures. The PDFs of apparent source temperatures for a cylindrical enclosure with and without considering reflections from the walls of the enclosure are shown in Fig. 19. The walls of the enclosure were assumed to absorb 20% of

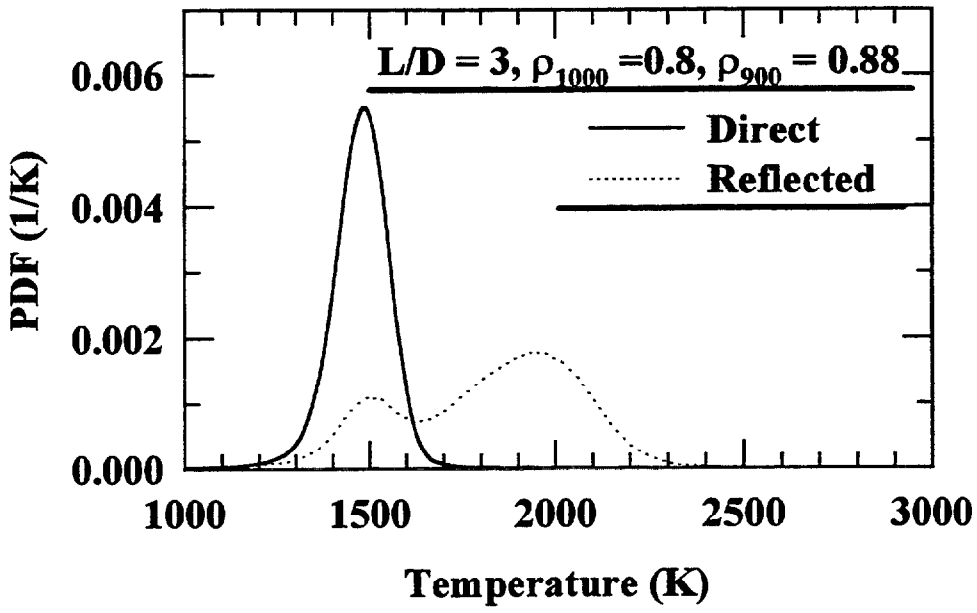

Figure 19. Effect of reflections on the apparent temperatures in a cylindrical enclosure.

the photons at 1000 nm, and 12% of the photons at 900 nm. The specularity of the reflectivity was also set at 0.4. A fraction of photons reaches the detector without undergoing any reflections from the wall. The apparent source temperatures estimated by the NIR fire detector from these photons are the same as those obtained from direct viewing of the fire. A greater number of photons reaches the detector after interaction with the walls. This interaction increases the apparent source temperatures estimated by the NIR fire detector since longer wavelength photons are preferentially absorbed. Therefore, the PDF of apparent source temperatures obtained is a combination of direct and reflected photons, as indicated by the bimodal PDF shown in Fig. 19.

The effect of the wall reflections on the PDF of apparent source temperatures for the rectangular enclosure is shown in Fig. 20. Similar to the results obtained within a cylindrical enclosure, the combination of direct and reflected photons result in a bimodal PDF for the apparent source temperatures estimated by the NIR fire detector.

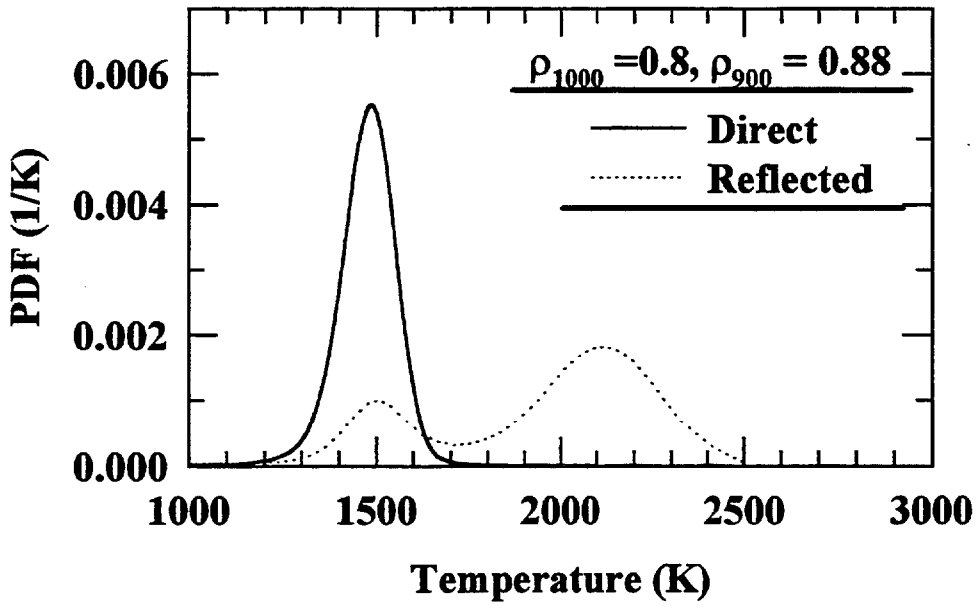

Figure 20. Effect of reflection on the apparent temperatures in a rectangular enclosure.

Despite the higher values for the estimated source temperatures in both cases, the NIR fire detector could successfully discriminate the fires from background radiation., since most of the temperatures are still within 800 to 2500 K. For a unit made of two rectangular shaped rooms, when the fire starts in one room, the above calculation will provide the joint PDF of intensities at the doorway to the other room, and also from the doorway to the any detector location. The present simulations helps to develop a design tool to optimally locate the fire detector in a multiple room enclosure.

4. Conclusions and Recommendations

A new type of near infrared (NIR) fire detector was developed and evaluated during the two year period covered by this grant. The major conclusions of the present study are:

(1) The normalized power spectral density of spectral radiation intensity at a near infrared wavelength and the apparent source temperatures obtained using two wavelength measurements are sufficient to determine the presence of open and smoldering fires.
(2) Open fires can be detected from direct as well as reflected radiation with very low false alarm rates using the NIR fire detector. Therefore, the NIR fire detector can be used for multiple room monitoring for open fires.
(3) Smoldering fires can be detected only from direct radiation, since the low temperatures associated with these fires resulted in very low radiation intensities at 900 and 1000 nm.
(4) The Discrete Probability Function (DPF) method in conjunction with a photon tracing algorithm was extended to treat specular and diffuse reflections and absorption in a three dimensional enclosure. The DPF method is more accurate than the Monte Carlo method for determining the radiation intensities incident on the NIR fire detector after multiple reflections of the photons with the walls of the enclosure.
(5) The DPF method can be used to optimize the location of a NIR fire detector, used for monitoring a multiple room enclosure.

The six specific recommendations for future work are:

(1) Characterize the spectral radiation intensities at other wavelengths (particularly in the infrared) with a view of developing a low false alarm rate fire detector that can monitor both open and smoldering fires in multiple room enclosures.
(2) After the optimum wavelengths for fire detection have been determined, continue the development of the algorithm to allow faster response times.
(3) Develop the DPF and other numerical technique for handling surface radiative heat transfer problems in other geometrical shapes.
(4) Study the various numerical techniques that can be used to link the results from simple geometrical shapes together so as to predict radiation behavior in multiple room enclosures.
(5) A Small Business Innovative Research (SBIR) program is necessary to develop a commercial prototype of this device. The requirements for commercialization include a fast programmable Digital Signal Processing (DSP) Chip, CAD designed casing for size optimization, and detector modification for current draw optimization.
(6) A second SBIR is needed for the inclusion of the DPF or Monte-Carlo based enclosure codes into architectural design software.

References

Bevans, J. T., and Edwards, D. K., (1965), "Radiation Exchange in an Enclosure with Directional Wall Properties," *J. Heat Transfer*, vol. 87, pp. 388-396.

Billings, R. L., Barnes, J. W., Howell, J. R., and Slotboom, O. E., (1991), "Markov Analysis of Radiative Transfer in Specular Enclosures," *J. Heat Transfer*, vol. 113, pp. 429-436.

Bobco, R. P., (1964), "Radiation Heat Transfer in Semigray Enclosures with Specularly and Diffusely Reflecting Surfaces," *J. Heat Transfer*, vol. 86, pp. 123-130.

Burgart, C. E., and Stevens, P. N., (1970), "A General Method of Importance Sampling the Angle of Scattering in Monte Carlo Calculations," *Nucl. Sci. Eng.*, vol. 42, pp. 306-323.

Burns, P. J., and Pryor, D. V., (1989), "Vector and Parallel Monte Carlo Radiative Heat Transfer Simulation," *Numerical Heat Transfer*, vol. 16, pp. 97-124.

Burns, P. J., Loehrke, R. I., Dolaghan, J. S., and Maltby, J. D., (1992), "Photon Tracing in Axisymmetric Enclosures," *Developments in Radiative Heat Transfer*, HTD-vol. 23, ASME, NY, pp. 93-99.

Burns, P. J., Maltby, J. D., and Christon, M. A., (1990), "Large-Scale Surface to Surface Transport for Photons and Electrons via Monte Carlo," *Computing Systems in Engineering*, vol. 1, pp. 75-99.

CEN, (1982) "Components of Automatic Fire Detection Systems: Fire Sensitivity Test," *Part 9, European Committee for Standardization*, Brussels.

Corlett, R. C., (1966), "Direct Monte Carlo Calculation of Radiative Heat Transfer in Vacuum," *J. Heat Transfer*, vol. 88, pp. 376-382.

Drost, M. K., and Welty, J. R., (1992) "Monte Carlo Simulation of Radiation Heat Transfer in Arrays of Fixed Discrete Surfaces using Cell-to-Cell Photon Transport," *Developments in Radiative Heat Transfer*, HTD-vol. 203, ASME, NY, pp. 85-91.

Eckert, E. R. G., and Sparrow, E. M., (1961), "Radiative Heat Exchange Between Surfaces with Specular Reflection," *Int. J. Heat Mass Transfer*, vol. 3, pp. 42-54.

Emery, A. F., and Carson, W. W., (1968), "A Modification to the Monte Carlo Method-The Exodus Method," *J. Heat Transfer*, vol. 90, pp. 328-332.

Gore, J. P., (1986), *A Theoretical and Experimental Study of Turbulent Flame Radiation*, Ph.D. Thesis, Pennsylvania State University, PA (1986).

Grosshandler, W. L., (1992) "An Assessment o Technologies for Advanced Fire Detection," *Heat and Mass Transfer in Fire and Combustion Systems*, HTD-223, ASME, NY pp. 1-9.

Haji-Sheikh, (1988), "Monte Carlo Methods," in *Handbook of Numerical Heat Transfer*, (Eds. W. J. Minkowsycz, E. M. Sparrow, G. E. Schneider and R. H. Pletcher), John Wiley & Sons Inc., New York.

Hall, J. R., (1989), "The Latest Statistics on U. S. Home Smoke Detectors," *Fire Journal*, vol. 83, pp. 39-41.

Hottel, H. C., (1954), "*Heat Transmission*", McGraw-Hill Book Co., New York, NY.

Howell, J. R., and Perlmutter, M., (1964), "Monte Carlo Solution of Thermal Transfer Through Radiant Media Between Gray Walls," *J. Heat Transfer*, vol. 86, pp. 116-122.

Howell, J. R., (1968), "Application of Monte Carlo to Heat Transfer Problems," *Advances in Heat Transfer*, vol. 5, Academic Press, NY, PP. 1-54

Kahn, H., and Marshall, A. W., (1953), "Methods of Reducing Sample Size in Monte Carlo Computations," *J. Operations Res. Society of America*, vol. 1 pp., 263-278.

Karter Jr., M. J., (1996), "NFPA's Latest Fire Loss Figures," *NFPA Journal*, vol. 90, pp. 52-59.

Lanore, J. M., (1971), "Weighting and Biasing of a Monte Carlo Calculation for Very Deep Penetration of Radiation," *Nucl. Sci. Eng.*, vol. 45, pp. 66-72.

Lin, S. H., and Sparrow, E. M., (1965), "Radiant Exchange Among Curved Specularly Reflecting Surfaces-Application to Cylindrical and Conical Cavities," *J. Heat Transfer*, Series C, vol. 87, pp. 123-130.

Luck, H. O., (1992) "Dedicated Detection Algorithms for Automatic Fire Detection," *Proceedings of the Third International Symposium on Fire Safety Science*, pp. 135-148.

Mahan, J. R., Kingsolver, J. B., and Mears, D. T., (1979), "Analysis of Diffuse-Specular Axisymmetric Surfaces with Application to Parabolic Reflectors," *J. Heat Transfer*, vol. 101, pp. 689-694.

Maltby, J. D., and Burns, P. J., (1991), "Performance, Accuracy, and Convergence in a three-dimensional Monte Carlo Radiative Heat Transfer Simulation," *Numerical Heat Transfer*, vol. 19, pp. 191-209.

Middleton, J. F., (1989), "Flame Detectors", *Ninth International Conference on Automatic Fire Detection*, AUBE-89, Duisburg, Germany, pp. 143-154.

Modest, M. F., (1978), "Three-Dimensional Radiative Exchange Factors for Non-Gray, Non-Diffuse Surfaces," *Numerical Heat Transfer*, vol. 1, pp. 403-416.

Naraghi, M. H. N, and Chung, B. T. F., (1984), "A Stochastic Approach for Radiative Exchange in Enclosures with Nonparticipating Medium," *J. Heat Transfer*, vol. 106, pp. 690-698.

Okayama, Y., Ito, T., and Sasaki, T., (1994), "Design of Neural Net to Detect Early Stages of Fire and Evaluation by Using Real Sensors' Data," *Proceedings of the Fourth International Symposium on Fire Safety Science*, pp. 751-759.

Oppenheim, A. K., (1956), "Radiation Analysis by the Network Method," *Trans. ASME*, vol. 78, pp. 725-735.

Parthasarathy, G., Patankar, S. V., Chai, J. C., and Lee, H. S., (1994), "Monte Carlo Solutions for Radiative Heat Transfer in Irregular Two Dimensional Geometries," *Radiative Heat Transfer: Current Research*, HTD-vol. 276, ASME, NY, pp. 191-199.

Perlmutter, M., and Howell, J. R., (1964), "Radiant Transfer Through a Gray Gas Between Concentric Cylinders Using Monte Carlo," *J. Heat Transfer*, vol. 86, pp. 169-179.

Rabl, A., (1977), "Radiation Transfer Through Specular Passages-A Simple Approximation," *Int. J. Heat Mass Transfer*, vol. 20, pp. 323-330.

Sarofim, A. F., and Hottel, H. C., (1966), "Radiative Exchange Among Non-Lambert Surfaces," *J. Heat Transfer*, vol. 88, pp. 37-44.

Shamsundar, N., Sparrow, E. M., and Heinish, R. P., (1972), "Monte Carlo Radiation Solutions-Effect of Energy Partitioning and Number of Rays," *Int. J. Heat Mass Transfer*, vol. 16, pp. 690-694.

Sivathanu, Y. R., and Faeth, G. M., (1990), "Temperature/ Soot Volume Fraction Correlations in Fuel-rich Region of Buoyant Turbulent Diffusion Flames," *Combust. Flame*, vol. 89, pp. 150-165.

Sivathanu, Y. R., Gore, J. P. and Dolinar, J., (1991), "Transient Scalar Properties of Strongly Radiating Jet Flames," *Combust. Sci. and Tech.*, vol. 76, pp. 45-66.

Sivathanu, Y. R., and Gore, J. P., (1991), "Simultaneous Multiline Emission and Absorption Measurements in Optically Thick Turbulent Flames," *Combust. Sci. and Tech.*, vol. 80, pp. 1-21.

Sivathanu, Y. R., and Gore, J. P., (1993), "A discrete probability function method for the equation of radiative transfer," *J. Quant. Spec. & Rad. Trans.*, vol. 49, pp. 269-280.

Sivathanu, Y. R., and Gore, J. P., (1994), "A Discrete Probability Function Method for Radiation in Enclosures and Comparison with the Monte Carlo Method," *Radiative Heat Transfer: Current Research*, HTD-vol. 276, ASME, NY, pp. 213-218.

Sparrow, E. M., Gregg, J. L., Szel, J. V., and Manos, P., (1961), "Analysis, Results and Interpretation for Radiation Between Simply Arranged Gray Surfaces," *J. Heat Transfer*, vol. 83, pp. 217-214.

Sparrow, E. M., Eckert, E. R. G., and Jonsson, V. K., (1962), "An Enclosure Theory for Radiative Exchange Between Specularly and Diffusely Reflecting Surfaces," *J. Heat Transfer*, vol. 84, pp. 294-300.

Tong, T. W., and Skocypec, D. R., 1992, "Summary on Comparison of Radiative Heat Transfer Solutions for a Specified Problem," *Developments in Radiative Heat Transfer*, HTD-vol. 203, ASME, NY, pp. 253-264.

Toor, J. S., and Viskanta, R. (1968), "A Numerical Experiment of Radiant Heat Interchange by the Monte Carlo Method," *Int. J. Heat Mass Transfer*, vol. 11, pp. 883-897.

Wetzork, J. M., Kern, M. T., and Shamrodola, K. A., (1992), "Fiber Optic Fire Sensor," *Fiber Optics and Laser Sensors X*, SPIE, vol. 1795, pp. 280-285.

NIST-114 (REV. 6-93) ADMAN 4.09

U.S. DEPARTMENT OF NATIONAL INSTITUTE OF STANDARDS AND TECHNOLOGY

MANUSCRIPT REVIEW AND APPROVAL

INSTRUCTIONS: ATTACH ORIGINAL OF THIS FORM TO ONE (1) COPY OF MANUSCRIPT AND SEND TO: WERB SECRETARY, BUILDING 820, ROOM 125

(ERB USE ONLY)	
ERB CONTROL NUMBER: G	DIVISION:
PUBLICATIONS REPORT NUMBER: NIST-GCR-98-747	CATEGORY CODE:
PUBLICATION DATE: April 1998	NO. PRINTED PAGES:

TITLE AND SUBTITLE (CITE IN FULL)
Fire Detection Using Reflected Near Infrared Radiation and Source Temperature Discrimination

CONTRACT OR GRANT NUMBER
60NANB5D0113

TYPE OF REPORT AND/OR PERIOD COVERED
NIST GCR 98-747

AUTHOR(S) (LAST NAME, FIRST INITIAL, SECOND INITIAL)
A.C. Lloyd, Y.J. Zhu, L.K. Tseng, J.P. Gore and Y.R. Sivathanu

PERFORMING ORGANIZATION (CHECK (X) ONE BOX)
- [ ] NIST/GAITHERSBURG
- [ ] NIST/BOULDER
- [ ] NIST/JILA

LABORATORY AND DIVISION NAMES (FIRST NIST AUTHOR ONLY)

SPONSORING ORGANIZATION NAME AND COMPLETE ADDRESS (STREET, CITY, STATE, ZIP)
Thermal Sciences & Propulsion Center, School of Mech. Engrg., Purdue University, West Lafayette, IN 47907

PROPOSED FOR NIST PUBLICATION

[ ] JOURNAL OF RESEARCH (NIST JRES)	[ ] MONOGRAPH (NIST MN)	[ ] LETTER CIRCULAR
[ ] J. PHYS. & CHEM. REF. DATA (JPCRD)	[ ] NATL. STD. REF. DATA SERIES (NIST NSRDS)	[ ] BUILDING SCI. SERIES
[ ] HANDBOOK (NIST HB)	[ ] FEDERAL INFO. PROCESS. STDS. (NIST FIPS)	[ ] PRODUCT STANDARDS
[ ] SPECIAL PUBLICATION (NIST SP)	[ ] LIST OF PUBLICATIONS (NIST LP)	[ ] OTHER
[ ] TECHNICAL NOTE (TN)	[ ] INTERAGENCY/INTERNAL REPORT (NISTIR)	[ ] —

PROPOSED FOR NON-NIST PUBLICATION (CITE FULLY): [ ] —U.S. FOREIGN— [ ]

PUBLISHING MEDIUM:	[ ] PAPER	[ ] DISKETTE	[ ] CD-ROM	[ ] WWW	[ ] OTHER

SUPPLEMENTARY NOTES

ABSTRACT (A 2000-CHARACTER OR LESS FACTUAL SUMMARY OF MOST SIGNIFICANT INFORMATION. IF DOCUMENT INCLUDES A SIGNIFICANT BIBLIOGRAPHY OR LITERATURE SURVEY, CITE IT HERE. SPELL OUT ACRONYMS ON FIRST REFERENCE.) (CONTINUE ON SEPARATE PAGE, IF NECESSARY.)

A new type of near infrared (NIR) fire detector which utilizes a statistical analysis of apparent source temperature of fires was developed. The characteristics of five standard test fires specified in the guidelines of the European Committee for Standardization were measured and utilized to develop a fire detection algorithm. The normalized power spectral density of the radiation intensity at 900 or 1000 nm combined with the PDF of the apparent source temperatures are sufficient to determine the presence of the test fires in the vicinity of the detector. When direct radiation is incident, four of the five test fires were always detected. The smoldering wood fire was detected only if the NIR fire detector was very close. A numerical technique based on the Discrete Probability Function (DPF) method in conjunction with a ray tracing algorithm was developed to handle radiative heat transfer problems in rectangular and cylindrical enclosures without participating media. The numerical evaluation confirmed that the detector can successfully detect fires from reflected radiation of its sensitivity is sufficiently high.

KEY WORDS (MAXIMUM OF 9; 28 CHARACTERS AND SPACES EACH; SEPARATE WITH SEMICOLONS; ALPHABETIC ORDER; CAPITALIZE ONLY PROPER NAMES)
Fire detection; infrared radiation; radiation heat transfer.

AVAILABILITY:
- [X] UNLIMITED
- [ ] FOR OFFICIAL DISTRIBUTION - DO NOT RELEASE TO NTIS
- [ ] ORDER FROM SUPERINTENDENT OF DOCUMENTS, U.S. GPO, WASHINGTON, DC 20402
- [X] ORDER FROM NTIS, SPRINGFIELD, VA 22161

NOTE TO AUTHOR(S); IF YOU DO NOT WISH THIS MANUSCRIPT ANNOUNCED BEFORE PUBLICATION, PLEASE CHECK HERE. [ ]